or Research Center
4-5000

DTRC-91/006 February 1991

Propulsion and Auxiliary Systems Department
Research and Development Report

Reflection of Incident Pressure Waves by Ribbed Panels

by
G. Maidanik and J. Dickey

DTRC-91/006 Reflection of Incident Pressure Waves by Ribbed Panels

MAJOR DTRC TECHNICAL COMPONENTS

CODE 011 DIRECTOR OF TECHNOLOGY, PLANS AND ASSESSMENT

12 SHIP SYSTEMS INTEGRATION DEPARTMENT

14 SHIP ELECTROMAGNETIC SIGNATURES DEPARTMENT

15 SHIP HYDROMECHANICS DEPARTMENT

16 AVIATION DEPARTMENT

17 SHIP STRUCTURES AND PROTECTION DEPARTMENT

18 COMPUTATION, MATHEMATICS & LOGISTICS DEPARTMENT

19 SHIP ACOUSTICS DEPARTMENT

27 PROPULSION AND AUXILIARY SYSTEMS DEPARTMENT

28 SHIP MATERIALS ENGINEERING DEPARTMENT

DTRC ISSUES THREE TYPES OF REPORTS:

1. **DTRC reports, a formal series,** contain information of permanent technical value. They carry a consecutive numerical identification regardless of their classification or the originating department.

2. **Departmental reports, a semiformal series,** contain information of a preliminary, temporary, or proprietary nature or of limited interest or significance. They carry a departmental alphanumerical identification.

3. **Technical memoranda, an informal series,** contain technical documentation of limited use and interest. They are primarily working papers intended for internal use. They carry an identifying number which indicates their type and the numerical code of the originating department. Any distribution outside DTRC must be approved by the head of the originating department on a case-by-case basis.

NDW-DTNSRDC 5602/50 (Rev. 2-88)

David Taylor Research Center
Bethesda, MD 20084–5000

DTRC–91/006 February 1991
Propulsion and Auxiliary Systems Department
Research and Development Report

Reflection of Incident Pressure Waves by Ribbed Panels

by

G. Maidanik and J.Dickey

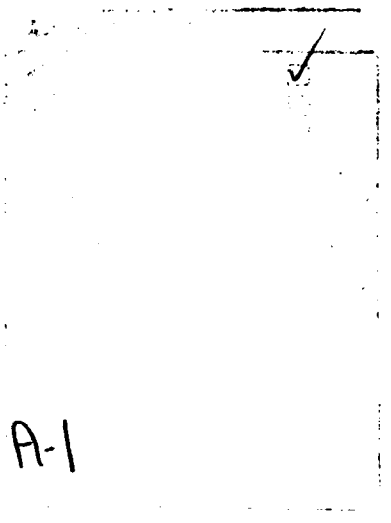

A-1

CONTENTS

ABSTRACT

The definitions of the reflection coefficients, in the absence of ribs and due to ribs, of an incident pressure wave on a plane at the surface of a ribbed fluid loaded panel are defined, examined, and computed. The incident pressure wave is described by a plane wave and by a collimated beam. The results of representative computations are displayed. Through these displays, some aspects of the influence on the reflection coefficients caused by changes in the parameters that describe the ribbed panel, the fluid loading, and the incidence are investigated. These aspects include wavenumber aliasings and symmetries in some of the terms and factors that compose the expressions for the reflection coefficients; the wavenumber of concern lies across the ribs. Aliasings are present, however, only when the separations between adjacent ribs are conditioned to be equal. Moreover, in some of these aliased terms and factors, symmetry is present only when the incidence obeys specific conditions. Disturbing either of these conditions tends to spoil the aliasing and/or the symmetries in these terms and factors. It is shown, however, that the aliasing and symmetry properties are invariant to changes in the parameters that describe the ribbed panel and/or the fluid loading to which it is subjected.

The role that the phenomenon of pass and stop bands (bands in reference to the frequency domain) plays in the reflection properties of ribbed fluid loaded panels is of particular interest here. It is illustrated that in the frequency ranges of pass bands, diffraction orders and aliasings tend to fade, and in the frequency ranges of stop bands they are enhanced. Fluid loading subdues the pass and stop bands; however, even substantial fluid loading does not eliminate these bands. Finally, the relationship between the reflection coefficients defined on the surface of the panel and on a control surface placed in the far-field is formulated and discussed.

ADMINISTRATIVE INFORMATION

This work was supported by the Ship Acoustics Department, Code 19, and the Propulsion and Auxiliary Systems Department, Code 27, of the David Taylor Research Center.

INTRODUCTION

Recently the authors developed a formalism to account for the response of a ribbed panel that may or may not be stratified by composite layers and which is subjected to external drives [1]. Herein the simplest model of a ribbed panel is considered and some aspects of the reflection of an incident pressure wave by its surface is explored. The formalism is cast in terms of the "impulse reflection function" $R_{11}(k \mid k', k_y \mid k_y', \omega \mid \omega')$ of the panel so that an incident pressure wave $P_{I1}(k', k_y', \omega')$ yields the reflected pressure wave $P_{R1}(k, k_y, \omega)$ in the form

$$P_{R1}(k, k_y, \omega) = \int R_{11}(k \mid k', k_y \mid k_y', \omega \mid \omega')\ dk'dk_y'd\omega'\ P_{I1}(k', k_y', \omega') \quad , \tag{1}$$

where the wave vector variable $\{k, k_y\}$ lies in the plane of the panel and is the Fourier conjugate of the spatial vector variable $\{x, y\}$, and the frequency variable ω is the Fourier conjugate of the temporal variable t, see Figs. 1 and 2. Both the incident pressure wave P_{I1} and the reflected pressure wave P_{R1} are pressures assessed in the fluid on a plane that is adjacent to the top surface of the panel. Quantities in reference to the top surface of the panel are designated by a unit subscript [1]. To assess the reflected pressure wave on a parallel control plane off the surface of the panel, a simple propagation process needs to be applied [1]. It is further noted that the spectral vector $\{k, k_y, \omega\}$ defines the reflected pressure wave. If the unribbed panel is uniform, the attached ribs are uniform, parallel, and lie in the y-direction, and the ribbed panel and its environment are temporally stationary, then

$$R_{11}(k \mid k', k_y \mid k_y', \omega \mid \omega') \rightarrow R_{11}(k \mid k', \varpi_2)\ \delta(k_y - k_y')\ \delta(\omega - \omega') \quad , \tag{2}$$

where $\varpi_2 = \{k_y, \omega\}$. Using Eq. (2), Eq. (1) reduces to

$$P_{R1}(k, \varpi_2) = \int R_{11}(k \mid k', \varpi_2)\ dk'\ P_{I1}(k', \varpi_2) \quad . \tag{3}$$

As expected, the integration remains only in the domain in which nonuniformities exist. It is

convenient to abbreviate Eq. (3) in the form

$$P_{R1}(k) = \int R_{11}(k \mid k')\ dk'\ P_{I1}(k') \quad . \tag{4}$$

where the spectral vector ω_7 is suppressed as obvious. This kind of abbreviation is extensively used in this paper. The functional form of $R_{11}(k \mid k')$ is derived in Reference 1 to be

$$R_{11}(k \mid k') = R_{011}(k)\ \delta(k-k') + R_{s11}(k \mid k') \quad , \tag{5}$$

where[1]

$$R_{011}(k) = \left[1 - Z_{1f}(k)\ \{2Y_{11}(k) + S_{1p}(k)\ G_{\infty}(k)\ 2S_{p1}(k)\}\right] \quad , \tag{6}$$

$$R_{s11}(k) = Z_{1f}(k)\ S_{1p}(k)\ G_s(k \mid k')\ 2S_{p1}(k') \quad . \tag{7}$$

The factors $G_{\infty}(k)$ and $G_s(k \mid k')$ combine in the form

$$G(k \mid k') = G_{\infty}(k)\ \delta(k-k') - G_s(k \mid k') \quad , \tag{8}$$

to yield the impulse response function of the ribbed panel so that the acceleration A(k) of the panel to an external drive $P_e(k')$ is obtained

$$A(k) = i\omega V(k) \quad ; \qquad V(k) = \int G(k \mid k')\ dk'\ P_e(k') \quad , \tag{9}$$

where V(k) is clearly the corresponding velocity of the panel. The factors $S_{1p}(k)$ and $S_{p1}(k)$ are transfer functions from the surface of the panel to the surface that is in contact with the fluid at the top, and vice versa, respectively [1]. The surface impedance $Z_{1f}(k)$ is that of the fluid atop the

---

[1]The opportunity is taken to issue an erratum to Eq. (39a) of Ref. 1. In the third term of the first of this equation, a factor of 2 was inadvertently omitted in front of the factor $S_{p\alpha}(k)$. Equation (7), in the text, stands corrected.

panel and, finally, $Y_{11}(k)$ is the (1,1)th element in the inverse of the surface impedance matrix describing the stratified (composite) panel; the layers are defined by lumped surface impedances and the panel itself is rendered blocked [1].

A BARE PANEL

In this paper a simple model is constructed of the ribbed panel. The model incorporates a bare panel. For such a model one obtains

$$Y_{11}(k) = 0 \quad ; \quad S_{1p}(k) = S_{p1}(k) = 1 \quad , \tag{10}$$

so that Eqs. (6) and (7) reduce to

$$R_{011}(k) = 1 - 2Z_{1f}(k)\ G_{\infty}(k) \quad , \tag{11}$$

$$R_{s11}(k \mid k') = 2Z_{1f}(k)\ G_{s}(k \mid k') \quad , \tag{12}$$

respectively. From Eqs. (5), (11), and (12) one obtains for this model

$$R_{11}(k \mid k') = [1 - 2Z_{1f}(k)\ G_{\infty}(k)]\ \delta(k-k') + 2Z_{1f}(k)\ G_{s}(k \mid k') \quad . \tag{13}$$

To derive the explicit form of $R_{11}(k \mid k')$ one needs to determine the explicit forms of $Z_{1f}(k)$, $G_{\infty}(k)$, and $G_{s}(k \mid k')$.

FLUID LOADED ISOTROPIC MEMBRANE-LIKE PANEL

In the model considered here, the panel is assumed to face a uniform fluid that occupies the semi-infinite space atop, and below a vacuum prevails; see Fig. 1. For such an environment

$$G_{\infty}(k) = [Z_{\ell}(k) + Z_{p}(k)]^{-1} \quad ; \quad Z_{\ell}(k) = Z_{t\ell}(k) + Z_{b\ell}(k) \quad ;$$

$$Z_{t\ell} = Z_{1f}(k) \quad ; \quad Z_{b\ell}(k) = 0 \quad , \tag{14}$$

where $Z_{lf}(k)$ is the surface impedance of the fluid in the plane of the panel

$$Z_{lf}(k) = (\rho\omega/k_3) \quad ; \quad |\underline{k}|^2 = k^2 + k_y^2 \quad ;$$

$$k_3 = \left[(\omega/c)^2 - |\underline{k}|^2\right]^{1/2} U\left[(\omega/c)^2 - |\underline{k}|^2\right] + i\left[|\underline{k}|^2 - (\omega/c)^2\right]^{1/2} U\left[|\underline{k}|^2 - (\omega/c)^2\right] , \quad (15)$$

and $Z_p(k)$ is the mechanical surface impedance of the uniform panel and Z_{ℓ} is the loading on the panel; $Z_{t\,\ell}$ on the top and $Z_{b\,\ell}$ on the bottom. In Eq. (15), ρ and c are the density and speed of sound of the fluid and U is the unit step function. It is further assumed that the unribbed (uniform) panel is membrane-like so that the mechanical surface impedance may be approximated in the form

$$Z_p(k) = i\omega m\left[1 - \{(k/k_p)^2 + (k_y/k_{py})^2\}\right] \quad ;$$

$$k_p = k_{p0}(1 - i\eta_p) \quad ; \quad k_{py} = k_{py0}(1 - i\eta_{py}) \quad , \quad (16)$$

where m is the mass per unit area and $\{k_p, k_{py}\}$ is the free wavevector of the panel. For a membrane responding in flexure or longitudinally

$$k_{p0} = (\omega/c_{\ell}) \quad ; \quad k_{py0} = (\omega/c_{\ell y}) \quad , \quad (17a)$$

in which $\{c_{\ell}, c_{\ell y}\}$ is the velocity of free wave propagation in the relevant type of the response and for a membrane simulating a plate responding in flexure

$$k_{p0}^2 = (\omega\,\omega_c/c)^2 \quad ; \quad k_{py0}^2 = (\omega\,\omega_{cy}/c^2) \quad , \quad (17b)$$

in which ω_c and ω_{cy} are the critical frequencies with respect to the speed of sound c of the fluid, in the x-domain and y-domain, respectively. A membrane-like panel cannot support a moment response. Thus, this choice for a panel greatly simplifies not only the expression for the mechanical surface impedance of the uniform pane but, more significantly, it simplifies the expression for the impulse response function $G_s(k \mid k')$ of the ribs. This function may then be stated in the form

$$G_s(k \mid k') = (2\pi)^{-1/2} \sum_n \sum_r G_\infty(k) \exp(ikx_n) R_n C_{nr} [G_\infty(k')/g_\infty] \exp(-ik'x_r) \quad , \quad (18a)$$

where

$$C_{nr} = \left(\delta_{ji} + \bar{g}_\infty(x_j - x_i)\ R_i(1 - \delta_{ji})\right)^{-1} \quad ;$$

$$\bar{g}_\infty(x_j - x_i) = [g_\infty(x_j - x_i)/g_\infty] \quad ; \quad g_\infty = g_\infty(\omega_2) = g_\infty(0, \omega_2) \quad ;$$

$$R_i = \bar{g}_i [1 + \bar{g}_i]^{-1} \quad ; \quad \bar{g}_i = (2\pi)^{-1/2} Z_i g_\infty \quad , \quad (19)$$

$$g_\infty(x_j - x_i) = (2\pi)^{-1/2} \int G_\infty(k)\ dk \exp[-ik(x_j - x_i)] \quad . \quad (20)$$

In Eqs. (18) through (20) x_n is the position in the x-domain of the (n)th rib; $g_\infty(x_j - x_i)$ is the line transfer admittance on the uniform panel from a line positioned at x_i to a line positioned at x_j; Z_i is the line impedance of the (i)th rib; and R_i is the reflection coefficient of the (i)th rib to an incident wave in the panel. Again, the dependence of quantities on the spectral vector ω_2 is suppressed [e.g., $R_i(\omega_2) = R_i$] as a matter of abbreviation. When the panel is regularly ribbed (i.e., when the ribs are identical, infinite in number, and the separations between adjacent ones are equal) Eq. (18) becomes

$$G_s(k \mid k') = G_\infty(k) [1 + \sum_j \tilde{H}_\infty(k + \kappa_j)]^{-1} \tilde{H}_\infty(k') \sum_n \delta(k + \kappa_n - k') \quad , \quad (21a)$$

where it is selected that $x_0 = 0$ and

$$|x_{n+1} - x_n| = b \quad ; \quad \kappa_j = j\kappa_1 \quad ; \quad \kappa_1 = (2\pi/b) \quad , \quad (22)$$

$$\tilde{H}_\infty(k) = (Z/b)\ G_\infty(k) \quad ; \quad Z_n = Z_j = Z \quad . \quad (23)$$

Since the panel and its environment are simplistic -- a bare panel that is fluid loaded from atop

only – one may dispense with the single and double subscripts of unity; e.g., in Eqs. (11) and (12), $R_{011} = R_0$, $R_{s11} = R_s$, and $Z_{1f} = Z_f$.

In Eq. (21a) the restriction that the panel needs to be membrane-like may be readily removed. Indeed, the modification that needs to be made in Eq. (21a) to accommodate a plate-like panel — a panel that can support a moment response — is that the equation for the mechanical surface impedance of the panel be extended to include the flexural response of a plate; namely,

$$Z_p(k) = i\omega m \left[1 - \{(k/k_p)^2 + (k_y/k_{py})^2\}^2\right] \quad , \tag{24}$$

and the surface impedance ratio $\tilde{H}_\infty(k)$ to include the line moment impedance Z_M of the ribs; namely,

$$\tilde{H}_\infty(k) = [(Z - ikZ_M)/b]\, G_\infty(k) \quad . \tag{25}$$

[cf. Eqs. (16) and (23), respectively, and References 2 and 3.] Removing the corresponding restrictions in the case of Eq. (18a) is more complicated [1,2].

FIRST ORDER MODELS

Situations arise in which models of ribbed panels may be devised in a manner that suppresses natural phenomena so that simplified descriptions are obtained. Situations of this kind may be instituted to derive a formalism from which approximations to more complicated descriptions may be initiated. However, these situations may also be instituted to derive a contrast with the corresponding more complicated descriptions so that phenomena of particular interest may be pin pointed [4,5]. The first order models considered here generally fall into the second category for the deployment of simplified models. In the first order models, all interactions among ribs are artificially removed [4]. The removal of all interactions, as specified, renders Eq. (18a) to be

$$G_s(k \mid k') = (2\pi)^{-1/2} \sum_n G_\infty(k)\, R_n\, [G_\infty(k')/g_\infty] \exp[ix_n(k-k')] \quad ; \quad R_{nr} = \delta_{nr} \quad , \tag{18b}$$

and renders Eq. (21a) to be

$$G_s(k \mid k') = G_\infty(k)\, [1 + \bar{g}_0]^{-1}\, \tilde{H}_\infty(k') \sum_n \delta(k + \kappa_n - k') \quad ; \quad \bar{g}_0 = \bar{g}_i \quad , \tag{21b}$$

where the quantities and parameters were just defined in the preceding sections. A few computations involving Eqs. (18b) and (21b) are carried out for contrast with those involving Eqs. (18a) and (21a), respectively; the latter set describes the more natural model.[2] [It is noted that the transition from Eq. (18b) to Eq. (21b), as the appropriate conditions of regularity are finally reached, is much simpler than the corresponding transition from Eq. (18a) to Eq. (21a); the transition in the former set is a snap.]

PLANE AND COLLIMATED BEAM OF INCIDENT PRESSURE WAVES

The pressure due to a plane incident wave on a control plane placed parallel to the surface of the panel may be stated in the form

$$P_I(k', \omega_2) = P_{I0}\, \delta(k' - k_I)\, \delta(k'_y - k_{yI})\, \delta(\omega' - \omega_I) \quad , \tag{26}$$

where

$$k_I = (\omega_I/c)\, \sin(\theta_I) \cos(\phi_I) \quad ; \quad k_{yI} = (\omega_I/c)\, \sin(\theta_I) \sin(\phi_I) \quad , \tag{27}$$

the angular vector $\{\theta_I, \phi_I\}$ defines the angles of incidence and ω_I is the tone of the wave, see

---

[2]It is to be understood that situations may be conceived in which a proper model and its corresponding first order model may, in the limit, coincide. For example, if the panel is assigned a point reacting surface admittance G_∞ that is independent of the wavenumber k, then the proper model and its corresponding first order model coincide. This subject matter is not pursued here any further.

Fig. 2. It may be convenient and instructive to employ also a collimated beam of incident pressure wave. In a simple case of collimation, the expression for $P_I(k', \omega_2)$ remains separable in the form

$$P_I(k', \omega_2') = P_{I0}\, F_x(k' - k_I)\, F_y(k_y' - k_{yI})\, F_t(\omega' - \omega_I) \quad , \tag{28}$$

where, for example,

$$F_\alpha(z) = \exp(-iq_\alpha z)\,(\pi z)^{-1} \sin(L_\alpha z/2) \quad ; \quad \alpha = x, y, \text{or } t \quad ; \quad q_\alpha = x_c, y_c, \text{or } -t_c \quad . \tag{29}$$

In Eq. (29), the constants x_c, y_c, and t_c indicate the "center of the coordinate" in the x–, y–, and t–domain, respectively; the lengths.L_x and L_y are the spatial apertures in the x-and y-direction, respectively, and the time L_t is the "temperal aperture" of the collimated beam. It is noted that

$$\exp(-iq_\alpha z)\,(\pi z)^{-1} \sin(L_\alpha z/2) \underset{L_\alpha \to \infty}{\longrightarrow} \delta(z) \quad , \tag{30}$$

so that if L_x, L_y, and L_t are carried to infinity, in the limit Eq. (28) approaches and becomes Eq. (26). It is noted that $F_\alpha(z)$ has the dimensionality of L_α. It is, therefore, convenient to define

$$\overline{F}_\alpha(z) = (2\pi/L_\alpha)\, F_\alpha(z) \quad ; \quad \overline{F}_\alpha(z)\ \delta(z) = \delta(z) \quad , \tag{31}$$

where $\overline{F}_\alpha(z)$ is a dimensionless quantity.

REFLECTION COEFFICIENTS DUE TO RIBS

If the plane incident pressure wave P_I is as stated in Eq. (26), then the reflected pressure wave P_R is derived from Eqs. (2), (4), and (5) in the form

$$P_R(k, \omega_2) = P_{I0}(\omega_{2I}) R(k \mid k_I, \omega_{2I})\ \delta(k_y - k_{yI})\, \delta(\omega - \omega_I) \quad , \tag{32a}$$

where

$$R(k \mid k_I, \mathcal{Q}_{2I}) = R_\infty(k \mid k_I, \mathcal{Q}_{2I}) + R_s(k \mid k_I, \mathcal{Q}_{2I}) \quad ;$$

$$R_\infty(k \mid k_I, \mathcal{Q}_{2I}) = R_0(k_I, \mathcal{Q}_{2I})\, \delta(k - k_I) \quad . \tag{33a}$$

Again, provided the dependence of quantities on $\mathcal{Q}_{2I}$ [$= \{k_{yI}, \omega_I\}$] is obvious, this dependence may be suppressed and the quantity be superscripted by I to indicate this specific dependence; e.g., $R_s(k \mid k_I, k_{yI}, \omega_I) = R_s^I(k \mid k_I)$. In this abbreviation, Eq. (32a) may be stated as

$$P_R(k, \mathcal{Q}_2) = P_{I0}\, R^I(k \mid k_I)\, \delta(k_y - k_{yI})\, \delta(\omega - \omega_I) \quad , \tag{32b}$$

where

$$R^I(k \mid k_I) = R_\infty^I(k_I) + R_s^I(k \mid k_I) \quad ; \quad R_\infty^I(k \mid k_I) \equiv R_0^I(k_I)\, \delta(k - k_I) \quad . \tag{33b}$$

The quantity $R_0^I(k_I)$ is commonly referred to as the specular reflection coefficient of the uniform panel. In the absence of ribs, this quantity may be defined in the form

$$\bar{R}_\infty^I(k_I \mid k_I) = (2\pi/L_x^\infty)\, R^I(k_I \mid k_I) \to R_0^I(k_I) \quad ; \quad R_s^I(k \mid k_I) \equiv 0 \quad , \tag{34}$$

where L_x^∞ is "the aperture" of the uniform panel in the x-domain. In analogy, the reflection coefficient $\bar{R}_s^I(k \mid k_I)$ in lieu of the ribs may be defined as

$$\bar{R}_s^I(k \mid k_I) = (2\pi/L_x')\, R_s^I(k \mid k_I) \quad , \tag{35}$$

where L_x' is the total aperture of the ribs; namely

$$L_x' = |x_P - x_N| = \sum_n (x_{n+1} - x_n) \quad . \tag{36}$$

In Eq. (36) x_P designates the position of one end-rib and x_N the position of the other end-rib. It is apparent that the normalization of $\bar{R}_\infty^I$ and $\bar{R}_s^I$ is usually different, except when the ribs span the

entire extent of the uniform panel; e.g., when the panel is regularly ribbed. However, even when the normalization is different, the estimation of the reflection in terms of the reflection coefficient does not cause any difficulty. Excepting specular reflection, the reflection is entirely described in terms of the reflection coefficient $\bar{R}_s^I(k \mid k_I)$ due to ribs. Indeed, in this paper many of the computed illustrations are centered on $\bar{R}_s^I(k \mid k_I)$ and the normalization stated in Eqs. (35) and (36) is then used.

The measure of incompatibility that besets the definition of the reflection coefficients, when the aperture of the ribs is finite, may be removed somewhat by using a collimated form for the incident pressure wave. Moreover, the use of this type of incident pressure wave may render the model phenomenologically more like to actual situations. For the purpose of this paper it suffices to introduce collimation in the x-domain only. (The generalization to include collimations in the y-domain and the t-domain can be readily introduced at a cost of some increase in cumbersomeness.) The incident pressure wave is thus stated in the form

$$P_I(k', \omega_2') = P_{I0}\, F_x(k' - k_I)\ \delta(k_y' - k_{yI})\ \delta(\omega' - \omega_I) \quad . \tag{37}$$

[cf. Eqs. (26) and (28).] From Eqs. (2), (4), (5), and (37), one obtains Eq. (32b) with

$$\begin{aligned} R_x^I(k \mid k_I) &= R_{0x}^I(k \mid k_I) + R_{sx}^I(k \mid k_I) \quad ; \\ R_{0x}^I(k \mid k_I) &= R_0^I(k)\, F_x(k - k_I) \quad ; \\ R_{sx}^I(k \mid k_I) &= \int R_s^I(k \mid k')\, dk'\, F_x(k' - k_I) \quad , \end{aligned} \tag{38}$$

replacing Eq. (33b). The reflection coefficient $\bar{R}^I(k \mid k_I)$ of the ribbed panel to an incident pressure wave of the form expressed in Eq. (37) is then simply

$$\begin{aligned} \bar{R}^I(k \mid k_I) \equiv \bar{R}_x^I(k \mid k_I) &= (2\pi/L_x)\, R_x^I(k \mid k_I) \quad ; \\ \bar{R}_{0x}^I(k \mid k_I) = (2\pi/L_x)\, R_{0x}^I(k \mid k_I) \quad &; \quad \bar{R}_{sx}^I(k \mid k_I) = (2\pi/L_x)\, R_{sx}^I(k \mid k_I) \quad . \end{aligned} \tag{39}$$

The term $\bar{R}^I_{0x}$ is the reflection coefficient in the absence of ribs and $\bar{R}^I_{sx}$ is the reflection coefficient due to ribs. In the formalism here developed, these terms can be so separated, which is a substantial simplification. It is observed that the reflection coefficient $\bar{R}^I_x(k \mid k_I)$, as defined in Eq. (38), is dependent on the structure of the incident pressure wave. The definition in Eq. (39) is particularly useful if $L_x = L'_x$, where L'_x is as stated in Eq. (36). In this case the aperture of the incident pressure wave matches the aperture of the ribs on the panel and, therefore, the normalizing apertures in the first and the second terms in the first of Eq. (38) are identical.

It is interesting to note that Eq. (38) may be alternately obtained. In this derivation one starts with Eq. (33) and proceeds to impose on this equation a filtering window in the x-domain. If the window is similar to that imposed on the plane incident pressure wave described in Eq. (37), Eq. (38) is derived from Eq. (33). In this alternate procedure, the physical interpretation of Eq. (38) is slightly modified. The modification is commensurate with that resulting from inserting a filter in the input versus inserting the same filter in the output.

EXPLICIT EXPRESSIONS FOR THE REFLECTION COEFFICIENTS AND COMPUTATIONAL PROCEDURES

Using Eqs. (12) and (35), and Eqs. (18a) and (18b) one obtains

$$\bar{R}^I_s(k \mid k_I) = \Lambda^I_\infty(k)\, \bar{\bar{R}}^I_s(k \mid k_I) \quad , \tag{40}$$

$$\Lambda^I_\infty(k) = Z^I_f(k)\, G^I_\infty(k) \quad . \tag{41}$$

$$\bar{\bar{R}}^I_s(k \mid k_I) = (8\pi)^{1/2} \left[G^I_\infty(k_I)/g^I_\infty L'_x \right] \begin{cases} \sum_n \sum_r R^I_n \; C^I_{nr} \exp\left[i\,(kx_n - k_I x_r) \right] , & \text{(42a)} \\ \sum_n R^I_n \exp\left[i x_n (k - k_I) \right] \quad , & \text{(42b)} \end{cases}$$

where Z^I_f, G^I_∞, g^I_∞, R^I_n, C^I_{nr}, and L'_x, are defined explicitly in Eqs. (14) through (20), and (36).

Using Eqs. (11) through (15), (21), (38), (39), and (41), one obtains

$$\bar{\bar{R}}^{I}_{x}(k \mid k_I) = \bar{\bar{R}}^{I}_{0x}(k \mid k_I) + \bar{\bar{R}}^{I}_{sx}(k \mid k_I) \quad , \tag{43}$$

$$\bar{\bar{R}}^{I}_{0x}(k \mid k_I) = [1 - 2\Lambda^{I}_{\infty}(k)]\, \bar{\bar{F}}_{x}(k - k_I) \tag{44}$$

$$\bar{\bar{R}}^{I}_{sx}(k \mid k_J) = \Lambda^{I}_{\infty}(k)\, \bar{\bar{\bar{R}}}^{I}_{sx}(k \mid k_I) \quad , \tag{45}$$

$$\bar{\bar{\bar{R}}}^{I}_{sx}(k \mid k_I) = 2 \sum_{n} \tilde{H}_{\infty}(k + \kappa_n)\, \bar{\bar{F}}_{x}(k + \kappa_n - k_I) \begin{cases} B^{I}_{s}(k) \quad , & (46a) \\ B^{I}_{0} \quad , & (46b) \end{cases}$$

$$B^{I}_{s}(k) = \left[1 + \sum_{j} \tilde{H}_{\infty}(k + \kappa_j)\right]^{-1} \quad ; \quad B^{I}_{0} = \left[1 + \bar{g}^{I}_{0}\right]^{-1} \quad . \tag{47a}$$

where Z^{I}_{f}, G^{I}_{∞}, $\tilde{H}^{I}_{\infty}$, $\bar{\bar{F}}^{I}_{x}$, and $\bar{g}^{I}_{0}$, are defined explicitly in Eqs. (14) through (17), (21) through (23), (31), and (39).

The dual representation of the reflection coefficients as expressed in Eqs. (40) and (42) and Eqs. (43) through (46) may assist in examining, among other features, the relationship between introducing the finiteness of the structure in terms a finite aperture of ribs, on the one hand, and in terms of a collimated incidence of a finite aperture on the other. However, comparing results issued by Eqs. (40) and (42) with those issued by Eqs.(43) through (46), one finds a fundamental difficulty. Equations (43) through (46) readily accounts for fluid loading; fluid loading in spectral space is, with the exception of the factor B^{I}_{0} in Eq. (46b), accounted for simply by an algebraic term in the surface admittance of the panel. On the other hand, the evaluation of the line transfer admittance $g_{\infty}(x_j - x_i)$, with fluid loading in place, presents a layer of computational difficulties. [cf. Eq. (20).] In this sense the evaluations of g^{I}_{∞} and R^{I}_{n} and, in particular, the evaluations of C^{I}_{nr} in Eq. (42) are cumbersome [6,7]. In order to afford a comparison between the computational

results of Eqs. (40) and (42) and those of Eqs. (43) through (45), without completely ignoring fluid loading in Eq. (42) and in B_0^I, it is necessary to modify this equation and B_0^I to accommodate some aspects of fluid loading even if only heuristically and over a limited range in the wavenumber-frequency (k–ω) domain. . Fluid loading may be largely accounted for by evaluating g_∞^I, R_n^I, and C_{nr}^I, which appear in Eq. (42), and by evaluating $\bar{g}_0$ in B_0^I, which appears in Eq. (45b), as if fluid loading is absent and then merely modifying, in these quantities, the mass per unit area m and the free wavenumber k_{p0} of the uniform panel as follows:

$$m \rightarrow m\,[1 + (\omega_c/\omega)^{1/2}\varepsilon_c] \quad ; \quad k_{p0} \rightarrow k_{p0}\,[1 + (\omega_c/\omega)^{1/2}\varepsilon_c]^{1/2} \quad . \tag{48}$$

[cf. Reference 3.] In this paper the reflection of a pressure wave by the surface of a ribbed panel is examined by performing computations of $\overline{R}_s^I\,(k\,|\,k_I)$, as stated in Eqs. (40) and (42), and of $\overline{R}_{sx}^I(k\,|\,k_I)$ and $\overline{R}_x^I(k\,|\,k_I)$, as stated in Eqs. (43) through (46). However, before starting computations the nature of a few individual factors in the expressions for these quantities need examining. This examination may help readers to decipher the subsequent displays of the computations of these quantities. Also, it may allow for a few observations of import to be made a priori. Such observations correspond to those already made in References 2 and 3, again emphasizing the basic significance and the common ground that the impulse response function plays in the formalism dealing with all the various responses of a structure. The various responses are generated, in the main, in consequence of differing drives to which the structure is subjected.

If the unribbed panel is subjected to an external drive $P_e^I(k)$, then the drive (pressure) $P_f^I(k)$ that the motion of the panel will generate on its surface is given by

$$P_f^I(k) = \Lambda_\infty^I(k)\,P_e^I(k) \quad . \tag{49}$$

This example may be used to interpret the physical meaning of $\Lambda_\infty^I(k)$ which appear in Eqs. (40), (41), (44), and (45). It is thus clear that $\Lambda_\infty^I(k)$ is, as is the specular reflection term, a property of

the uniform panel; the ribs do not influence this factor. It is noted that $Z_f^I(k)$ and $G_\infty^I(k)$, as stated in Eqs. (14) through (25), are symmetric in k and, therefore, so is $\Lambda_\infty^I(k)$; that is

$$Z_f^I(k) = Z_f^I(-k) \quad ; \quad G_\infty^I(k) = G_\infty^I(-k) \quad ; \quad \Lambda_\infty^I(k) = \Lambda_\infty^I(-k) \quad . \tag{50}$$

[cf. Eq. (41).] Typical characteristics of $\Lambda_\infty^I(k)$ are illustrated in Fig. 3. In this figure the magnitude of $\Lambda_\infty^I(k)$ is displayed as a function of the normalized wavenumber (k/κ_1), where κ_1 is a wavenumber scale factor. In Fig. 3 the frequency is fixed at $(\omega_I/\omega_c) = 0.4$, the angle ϕ_I of incidence is fixed at zero; $k_{yI} = 0$, and the panel is membrane-like and isotropic; $k_p = k_{py}$, with k_{p0} as specified in Eq. (17b) and the mechanical loss factor η_p is set at 0.005. In Fig. 3a the fluid loading parameter ε_c is fixed at 0.1 and in Fig. 3b, at 0.001. Of interest are the peaks at the sonic and at the free wavenumbers; at the sonic wavenumber, $\Lambda_\infty^I(k) = 1$. The ridges associated with the peaks at the sonic wavenumber are more prominent when the value of the fluid loading parameter is lower. On the other hand, the free wavenumber decreases as the fluid loading is decreased. Beyond the free wavenumber, the magnitude of $\Lambda_\infty^I(k)$ diminishes quickly with increase in the wavenumber (k/κ_1); the mechanical surface impedance of the panel increases and the fluid loading decreases with increase in the wavenumber beyond the free wavenumber. The symmetry of $\Lambda_\infty^I(k)$ in k is evidenced in Fig. 3.

The factors $\overline{\overline{R}}_s^I(k \mid k_I)$ and $\overline{\overline{R}}_{sx}^I(k \mid k_I)$ are influenced directly and critically by the properties of the ribs; this is in addition to their dependence on the properties of the panel. Examining the factor $\overline{\overline{R}}_{sx}^I(k \mid k_I)$ first, it is noted that this quantity is aliased in k with respect to the harmonics $\kappa_j (= j\kappa_1)$ of the separation wavenumber κ_1 between adjacent ribs; $\kappa_1 = (2\pi/b)$. This aliasing is defined by

$$\overline{\overline{R}}_{sx}^I(k \mid k_I) = \overline{\overline{R}}_{sx}^I(k + \kappa_\tau \mid k_I) \quad . \tag{51a}$$

Typical characteristics of this factor are illustrated in Fig. 4, where the magnitude of $\overline{\overline{R}}_{sx}^I(k \mid k_I)$,

stated in Eq. (46), is displayed as a function of the normalized wavenumber (k/κ_1) with the normalized frequency (ω_I/ω_c) fixed at 0.4, the angle ϕ_I of incidence fixed at zero; $k_{yI} = 0$, the panel is membrane-like and isotropic; $k_p = k_{py}$, the free wavenumber k_{p0} is specified in Eq. (17b) and the mechanical loss factor η_p is set at 0.005; the line impedance of the ribs is assumed to be mass controlled; $Z_j = Z = i\omega M$, with (M/bm) set at 0.3, the separations between adjacent ribs is fixed at $(b\omega_c/c) = 16$, the aperture in the collimated incident pressure wave is 20b, and the fluid loading parameter ε_c is fixed at 0.1. In Figs. 4a and b Eq. (46a) is employed with $\theta_I = 0.9$ and zero, respectively. In Fig. 4c Eq. (46b) is employed with $\theta_I = 0.9$. The aliasing of $\overline{\overline{R}}^I_{sx}(k \mid k_I)$ in k is clearly apparent in Fig. 4.[3] In Fig. 4b, in addition, the factor $\overline{\overline{R}}^I_{sx}(k \mid k_I)$ is symmetric. Indeed, this factor is symmetric whenever $k_I = n\kappa_1$; namely

$$\overline{\overline{R}}^I_{sx}(k \mid k_I) = \overline{\overline{R}}^I_{sx}(-k \mid k_I) \quad ; \quad k_I = n\kappa_1 \quad . \tag{52a}$$

[It is noted that $\Lambda^I_\infty(k)$ is symmetric in k as specified in Eq. (50); however, this quantity is not aliased in k. Consequently, the reflection coefficients due to ribs are not aliased; i.e., neither $\overline{R}^I_{sx}(k \mid k_I)$ nor $\overline{R}^I_s(k \mid k_I)$ is aliased, whether $\overline{\overline{R}}^I_{sx}(k \mid k_I)$ or $\overline{\overline{R}}^I_s(k \mid k_I)$ are aliased or not.] Features of interest in Fig. 4 are the peaks at the diffraction orders (including the zeroth). In Fig. 4b the zeroth diffraction order is located at $(k/\kappa_1) = 0$, and symmetry, and not only aliasing, reigns. It is observed that Figs, 4a and c differ with respect to the wavenumber variable k. This difference is completely accounted for by the factor $B^I_s(k)$, which, in turn, accounts completely for the wavenumber dependence of the interactions among the ribs. (It is noted that the factor B^I_0 is independent of the wavenumber k.) The factor $B^I_s(k)$ is clearly aliased and symmetric in k; namely

---

[3]The general values, aliasings, and symmetries shown in the displays of the computations performed in this paper are valid only to within the finiteness of the samples and the rounding errors that are built into the computer program employed in the calculations and in the graphical presentations.

$$B_s^I(k) = B_s^I(-k) = B_s^I(k + \kappa_\tau) \quad . \tag{53}$$

Figure 4d depicts the magnitude of the factor $B_s^I(k)$, stated in Eq. (47a), as a function of the normalized wavenumber (k/κ_1) for the corresponding conditions and parametric values used in Fig. 4a. Interesting features are the considerable excursions in the values of $B_s^I(k)$ as a function of (k/κ_1). Yet, the aliasing and the symmetry in k are clearly visible. Close observation indicates that $B_s^I(k)$ substantially accounts for the differences in Figs. 4a and c. The more profound significance of this factor is subsequently discussed .

The factor $\overline{\overline{R}}_s^I(k \mid k_I)$ is examined next. In general, this factor is neither aliased nor symmetric in k. However, if the separations between adjacent ribs are equal then $\overline{\overline{R}}_s^I(k \mid k_I)$ is aliased in k; i.e.,

$$\overline{\overline{R}}_s^I(k \mid k_I) = \overline{\overline{R}}_s^I(k + \kappa_\tau \mid k_I) \quad ; \quad |x_{n+1} - x_n| = b \quad . \tag{51b}$$

[cf. Eq. (51a).] Moreover, if the incidence wavenumber k_I is harmonic in κ_1 then the factor $\overline{\overline{R}}_s^I(k \mid k_I)$ is also symmetric in k; i.e.,

$$\overline{\overline{R}}_s^I(k \mid k_I) = \overline{\overline{R}}_s^I(-k \mid k_I) \quad ; \quad |x_{n+1} - x_n| = b, \quad k_I = n\kappa_1 \quad . \tag{52b}$$

[cf. Eq. (52a).] Figure 5 shows typical characteristics of this factor . In this figure the magnitude of $\overline{\overline{R}}_s^I(k \mid k_I)$, stated in Eq. (42), is displayed as a function of the normalized wavenumber (k/κ_1) with the normalized frequency (ω_I/ω_c) fixed at 0.4; the angles θ_I and ϕ_I of incidence of a plane pressure wave are fixed at 0.9 and zero, respectively; the panel is membrane-like and isotropic; $k_p = k_{py}$, the free wavenumber k_{p0} is specified in Eq. (17b) and the mechanical loss factor η_p is set at 0.005, the line impedance of the ribs are assumed to be mass controlled; $Z_j = Z = i\omega M$, with (M/bm) set at 0.3, where b is a typical (averaged) separation between adjacent ribs and $(b\omega_c/c) =$ 16, the aperture is 21 ribs (= 20b), and the fluid loading parameter is fixed at 0.1 and Eq. (48) is

applied. In Fig. 5a the variations in the separations between adjacent ribs are randomly selected but not to exceed 0.1b. In Fig. 5b the separations between adjacent ribs are selected to be equal. Features of interest are the lack of aliasing, especially at the higher wavenumber range, shown in Fig. 5a. Also of interest is the favorable comparison between the prominences in Fig. 5b and the corresponding prominences in Fig. 4a.[3]

From the nature of Eqs. (40) through (47) in the formalism here developed, it emerges that changes in the parameters that define the uniform panel, the fluid loading, the separation wavenumber of the uniform ribs, and the incident pressure wave do not cause modifications in the aliasing and the symmetry of the quantities and factors that describe the reflection coefficients. The invariance of symmetry and aliasing, however, is limited to the particular models of the structure and to the uniformity of the environmental loading. As Eq. (38) indicates, even within the confine of simplified models, there are models for which this invariance may not be relevant. With this final observation attention is now turned to a more thorough examination of the nature of the reflection coefficients of ribbed panels immersed in uniform fluids.

COMPUTATIONS AND DISPLAYS OF THE REFLECTION COEFFICIENTS

The computations of the reflection coefficients performed and displayed herein are by no means exhaustive of either the capabilities of the formalism or the interest; they are merely representative. Thus, the quantities and parameters that describe the uniform panel and the ribs are kept simple, for the most part, ; e.g., the line impedances of the ribs are considered to be mostly mass controlled [2, 3]. It follows that the displays exhibit only some of the features in the reflection coefficients. In addition, only the magnitudes of these quantities are shown. These magnitudes are displayed as functions of the normalized wavenumber (k/κ_1) at successive and equal increments of the normalized frequency (ω_1/ω_c) for a number of fixed values of $(k_1 \mid \kappa_1)$. [It is noted that $(k_{y1}/k_1) = \tan(\phi_1)$.] To reduce the information in the displays, only prominences are exhibited; this is achieved by clipping the magnitudes by a threshold. In the displays here

presented, the threshold t^0 is a constant number assigned to each figure. The format of such computations and displays was adopted in recent papers by the authors. In these papers the response of ribbed panels that are driven by external mechanical line drives are described [2,3]. Nonetheless, the format is akin and suitable to be used for the purposes of this paper. Here then this format is standard. It is more usual to confine displays of the reflection coefficients only to the supersonic region of the spectral domain. This region is defined by $(k^2 + k_{yI}^2) < (\omega_I/c)^2$. Moreover, often only the evaluations of the peaks at the specular and the diffraction orders are of concern [4]. The displays presented in Figs. 6 through 10 cover the lower wavenumber portions of the subsonic regions as well as the entire supersonic regions. In addition, the distributions, – not just the peaks – of the prominences in the reflection coefficients are displayed. Included in these displays are prominences that are not strictly of the diffraction orders . These prominences are induced by the excitation of the structural resonances that are excited, on the one hand, by the spectral distributions in the incident pressure waves and, on the other, by the wavenumber conversion induced by the ribs for the ribs. The prominences at the spectral region defined by the free wavenumber in the panel and their aliasings, generated by the periodicity in the spacing of the ribs, are of particular significance in this category [2,3].

To avoid repetitions in the figure captions and to help with the interpretation of and comparison between figures, it is convenient to set standard conditions and values of quantities and parameters so that only deviations from these standards need be specified. Thus, the standard panel is an isotropic membrane that simulates the response of a plate responding in flexure; namely,

$$k_p = k_{py} \quad ; \quad k_p = k_{p0}(1 - i\eta_p) \quad ; \quad k_{p0}^2 = (\omega\omega_c/c^2) \quad ; \quad \omega_c = \omega_{cy} \quad .$$

The standard loss factor η_p of the membrane is equal to 0.005, the standard free wavenumber k_c $[=(\omega_c/c)]$ at the critical frequency is set equal to $(bk_c) = 16$; the separations between adjacent ribs

are equal and designated by b, the standard fluid loading parameter $\epsilon_c[= (\rho c/\omega_c m)]$ is equal to 0.1; the standard line impedances of the ribs are equal, $Z_j = Z$, and are mass controlled, $Z = i\omega M$, with $(M/bm) = 0.3$; the standard angles $\{\theta_I, \phi_I\}$ of incidence are equal to $\{0.9, 0\}$; and the standard aperture is 20b which typically spans 21 ribs. The standard coverage in the wavenumber-frequency domain is extended over the range $-1.5 \lesssim (k/\kappa_1) \lesssim 3.0$ and $0 < (\omega_I/\omega_c) \lesssim 0.6$. [cf. Figs. 3 through 5.]

Figure 6a displays the magnitude of the reflection coefficient $\overline{R}_s^I(k\,|\,k_I)$ in the standard format and under the standard conditions for a first order model of the ribbed panel. [cf. Eq. (42b) and (47).] The diffraction orders are clearly discernible, as is the scattering of the incident pressure wave into (subsonic) components that drive the (resonance) free waves in the panel. In this case the free waves are dispersive as stated in Eq. (17b). This dispersion is readily recognized in Fig. 6a when the free waves are compared with the negative first order diffraction loci. Both prominences that are associated with the diffraction orders and the free waves will be absent in the absence of ribs; see Eq. (33b). Figure 6b displays the magnitude of the reflection coefficient $\overline{R}_s^I(k\,|\,k_I)$ in the standard format and under the standard conditions for a proper model of the ribbed panel. A major difference between Figs. 6a and 6b emerges. In Fig. 6b the phenomenon of "pass and stop bands" is outstanding; this phenomenon is directly related to the full interactions among the regularly spaced ribs [5]. Clearly, in a pass band the influence of the ribs is faded, and enhanced in a stop band . The fadings and the enhancements are not confined to the diffraction orders, but to all the forms of scatterings; e.g., to the generation of the free waves and the aliasings thereof. The influence of the pass and stop bands on the reflective properties of ribbed panels are thus reminiscent of the influence of this phenomenon on the response of ribbed panels to localized drives [2,3]. In the former the "drive" is localized in the wavenumber domain (k–domain) and in the latter in the spatial domain (x–domain). The pass and stop bands manifest characteristics of the ribbed panel, be it excited by one drive form or another. The reminiscence is expected. Fig. 6c displays the effect of introducing a 10% randomly selected variations in the separations between

adjacent ribs; $(\Delta b/b) \lesssim 10^{-1}$, where Δb is a typical variation in the separation between adjacent ribs. The spoiling, by these variations, of the pass and stop bands and the aliasing is demonstrated in this figure, notwithstanding that only the low wavenumber range, namely $(k\Delta b)^2 \lesssim 1$, is used in the display.[4] The spoiling is severe in the higher wavenumber range, where $(k\Delta b)^2 > 1$, and the spoiling is more severe the higher the inequality. [cf. Fig. 5a.]

Figures 7a and b correspond to Fig. 6b except that in these two figures the normalized wavenumber at the critical frequency is changed from that of the standard value of $(bk_c) = 16$ in Fig. 6b, to $(bk_c) = 8$ and $(bk_c) = 24$, respectively. This change is commensurate with a change in the separation b between two adjacent ribs and a corresponding change in the mass per unit length M of the ribs so that (M/bm) is maintained at the standard value of 0.3 [2]. To maintain a decor, the normalized wavenumber scale is appropriately changed in Figs. 7a and b. The observed changes born by these figures as compared with Fig. 6b, are as expected.

Figures 8a and b display the results of computing the magnitude of $\overline{R}^I_{sx}(k|k_I)$ in the standard format and under standard conditions for a first order model and a proper model of a ribbed panel, respectively. Figure 8a should then be comparable with Fig. 6a, and Fig. 8b with Fig.6b. Clearly major correspondence is found in these comparisons. However, some details do not correspond in these comparisons. What is different in the two sets of descriptions of the panels and the incident pressure waves that may contribute to the observed disparities? In the first set, Figs. 6a and b, the aperture is related to the finite number of ribs; beyond this aperture the

---

[4]The aliasing in k is a phenomenon that is wavenumber (and, therefore, also spatially in x) related. On the other hand, the pass and stop bands is a phenomenon that is often viewed as frequency related. However, as is apparent from comparison of Eqs. (42a) and (46a) with Eq. (42b) and (46b), the interactions among the ribs are wavenumber k (and, therefore, also spatially x) dependent; e.g., the factor $B^I_s(k)$ versus the factor B^I_0. Indeed, the spatial regularity that is essential to the phenomenon of aliasing is also essential in these interactions for the phenomenon of pass and stop bands to arise. Thus, disturbing the regularity of the separations between adjacent ribs is bound to influence both these phenomena. In this sense the two phenomena are related.

panel is bold of ribs. In the second set, Figs. 8a and b, the aperture is related to the incident pressure wave and beyond this aperture the panel is regularly studded with ribs. It is thus not surprising that details do not correspond in the two sets, even if the quantities displayed are in terms of magnitudes and prominences, notwithstanding that the absence of pass and stop bands in Fig. 8a is recovered in Fig. 8b, as is the case with respect to Figs. 6a and b, respectively. The interactions among ribs that are regularly separated give rise to the phenomenon of pass and stop bands which in turn are clearly visible in the reflections and scatterings that are caused by the ribs [5].

Figure 9a displays in the standard format the co nputational results of the magnitude of the reflection coefficient $R^{I}_{0_x}(k\,|\,k_I)$ in the absence of ribs, as stated in Eq. (44), for the standard angles of incidence; $\{\theta_I, \phi_I\} = \{0.9, 0.0\}$. It shows that the distribution with respect to the normalized wavenumber (k/κ_1) is fairly wide and contains even subsonic components of significant magnitudes. Of course, the distribution in the reflection in the absence of ribs bears a factorial correspondence to the distribution in the incident pressure wave. Indeed, the distribution is largely determined by the normalized aperture function $\overline{F}_x(k-k_I)$ in Eq. (44). It is observed that whereas the incident pressure wave with respect to Fig. 6 is highly localized in the k-domain, with respect to Fig. 8, it is broad and contains significant components even in the subsonic range. In this sense the remark made with respect to the lack of detailed correspondence between Figs. 6 and 8 is further strengthened. Indeed, some of the discrepancies in details between Figs. 6 and 8 may be explained taking account of these very differences in the respective incident pressure waves. [cf. Section V.] In Figs. 9b, c, and d the standard angles of incidence are changed from {0.9, 0.0} to {0.3, 0.0}, {0.9, 0.3}, and {0.3, 0.3}, respectively. Of particular interest are Figs. 9c and d, where the introduction of a none-zero ϕ_I is accommodated. The results of this introduction conform to expectation.

Figure 10 displays in the standard format the magnitude of the reflection coefficient $\overline{R}^{I}_{x}(k\,|\,k_I)$ for three of the four incident pressure waves that are covered in Fig. 9. A comparison of

Fig. 10a with Fig. 8b illustrates the influence of including the reflection in the absence of ribs in the displays. The changes that occur with changes in the incidence angles may be deduced from comparisons of Fig. 10a with Figs. 10b and c. A point of interest is that the peaks at and in the vicinity of the specular angles are influenced by the reflection coefficients due to ribs indicating that the zeroth order diffraction by the ribs may be significant. The significance, however, varies with frequency.

There are many more issues that arise in the investigation of the reflective properties of ribbed structures. It may be proper to discuss a number of these issues in this paper. The purpose is to show that such issues can be conveniently and further addressed within the realm of the formalism and computational procedures herein developed. The issues to be singled out and briefly discussed are related to the effects that are associated with changes in aperture, with focussing and extension of the ranges displayed, with fluid loading, and, finally, with reflection to the far-field.

APERTURE EFFECTS

The larger the aperture the sharper are the distributions in the reflection and response, as a function of the wavenumber that lies in the direction of the aperture. Figure 11 illustrates this statement. This figure repeats Fig. 10a with a change in the aperture from its standard value of 20b ($\equiv$ 21 ribs) to 42b ($\equiv$ 43 ribs). Comparing Fig. 11 with Fig. 10a indeed illustrates the increase in sharpness of the distributions of the reflection coefficients defined in Eqs. (43) through (46).

FOCUSSING AND EXTENSION OF THE DISPLAYED RANGES

The displayed figures (Figs. 6 through 11) are limited to the standard wavenumber - frequency range defined by $-1.5 \lesssim (k/\kappa_1) \lesssim 3.0$ and $0 < (\omega_I/\omega_c) \leq 0.6$. An occasion may arise in which one may wish to focus the display on a specific sub-range. In Fig. 12a the display focuses on the sub-range $-.75 \lesssim (k/\kappa_1) \lesssim 1.5$ and $0 < (\omega_I/\omega_c) \leq 0.06$ of Fig. 10a. The focussing

increases the details in the reflection coefficient that pertain to the selected sub-range. On the other hand, an occasion may arise in which one may desire to display the reflection coefficient more extensively than is displayed in a standard figure. Figure 12b extends the display depicted in Fig. 10a from its standard range to the wavenumber-frequency range defined by $-3.0 \lesssim (k/\kappa_1) \lesssim 6.0$ and $0 < (\omega_1/\omega_c) \lesssim 2.4$. Of particular interest is the extension into the frequency above the critical frequency; i.e., into the frequency range $(\omega_1/\omega_c) \gtrsim 1$. In this range the free waves in the panel approach and become supersonic. The process of taking the free waves from just below the sonic range to that above it is compounded but of special interest. Such specific considerations are, however, beyond the scope of this paper. Again, the purpose is merely to point out that such considerations lie within the realm of the formalism and within the computational capabilities employed herein.

FLUID LOADING EFFECTS

Fluid loading effects on the reflective properties, in particular, and on the response properties, in general, are of interest to the investigation of the vibro-acoustics of ribbed panels. Many questionable rule-of-thumbs exist in this regard. Can the reflective and response properties of ribbed panels be estimated by ignoring fluid loading in some, but not in other, terms and factors in the formalism that accounts for these properties? Does fluid loading dull the sharpness of the patterns of the prominences (and valleys) in the displays of the reflection and response quantities of ribbed panels? Does fluid loading effects favor supersonic and disfavor subsonic components in these quantities? In what manner does fluid loading influence the phenomenon of pass and stop bands? Obviously, the answers to these and other relevant questions cannot be given within this paper. However, an attempt will be made to illustrate elements that may be involved in formulating these kind of questions and providing such answers.

It is apparent that some of the discrepancies in details between Figs. 6 and 8 are related to the fact that whereas fluid loading is introduced cavalierly and heuristically in the computations

leading to Fig. 6 via Eq. (48), in the computations leading to Fig. 8, fluid loading is properly accounted for. The measure of the influence of fluid loading on the reflective properties of a ribbed panel is made clear by comparing Figs. 6b and 8b with Figs. 13a and b, respectively. In the latter set of figures, the fluid loading parameter ε_c and, by necessity, also the threshold t^0, are changed from the standard values of 0.1 and 0.03, respectively, to 0.001 and 0.001, respectively. The changes in the patterns in the two sets of figures are clearly significant However, these changes can be readily accounted for; e.g., the observed decrease in the free wavenumber k_{p0}, as one proceeds from Fig. 6b to Fig. 13a, is as specified in Eq. (48). The corresponding decrease in k_{p0}, as one proceeds from Fig. 8b to Fig. 13b is more naturally, but less explicitly, accounted for. It is interesting that, by and large, the correspondence between Figs. 13a and b is better than that between Figs. 6b and 8b. The ridge at the sonic loci, which is more visible in Fig. 13b than in Fig. 13a, is not an artifact. It is governed by the factor $\Lambda^I_\infty(k)$, stated in Eq. (41) and relevantly illustrated in Fig. 3. [cf. the next section and Ref. 6.] The prominences in the reflection coefficients illustrated in Fig. 14 are computed with fluid loading only partially accounted for. In this figure the fluid loading is accounted for only in the factor $\Lambda^I_\infty(k)$, in Eqs. (42a) and (46a); in the remaining factors fluid loading is neglected; namely, ε_c is set equal to zero in $\overline{\overline{R}}^I_s(k \mid k_I)$ and $\overline{\overline{R}}^I_{sx}(k \mid k_I)$, stated in Eqs. (40) and (45a), respectively. The comparison between Figs. 14a and b is reminiscent of that between Figs. 6b and 8b, or even between Figs. 13a and b, respectively. It is observed that the specified neglect of fluid loading does not undermine the overhaul correspondence between Figs. 14a and b; except for details, the patterns in these figures are fairly identical. However, comparison between Figs. 6b and 13a and Fig. 14a, and between Figs. 8b and 13b and Fig. 14b indicate the dangers that beset the partial negligence of fluid loading in these specific and other manners. In the first comparisons, between Figs. 6b and 8b, and Fig. 14, the free wavenumber appears satisfactory, but not the positions of the pass and stop bands. In the second comparisons, between Figs. 13a and 13b, and Fig. 14, the situation is the reverse of the first. Again, it is noted that except for details, Figs. 14a and b bear between them a resemblance as

good as the resemblances between Figs. 6b and 8b and Figs. 13a and b, respectively. Thus, there are partial and mixed agreements and disagreements; hence, the caution for the dangers.

The comparisons between the various figures and set of figures that the reader was asked to perform were not simple, primarily because each figure contained a large volume of information. Some relief is provided by employing thresholds; further relief is afforded by the similarities of the patterns in the compared figures. Will it not be useful and of interest to investigate the influence of fluid loading on major characteristics of the reflective (and the response) properties of ribbed panels without the clutter of excessive information? An opportunity for such an investigation lies in Eq. (47a). It is noted that the factor $\overline{B}_s^I(k)$, defined by

$$\overline{B}_s^I(k) = B_s^I(k)\,[B_0^I]^{-1} \quad , \tag{47b}$$

accounts completely for the interactions among the ribs, and hence, in turn, the description of the pass and stop bands lie completely within this quantity, despite that not all the interactions among the ribs contribute directly to the phenomenon of pass and stop bands [5]. One may then use $\overline{B}_s^I(k)$ to investigate the extent and the manner by which fluid loading may influence the pass and stop bands, notwithstanding that this quantity is locked into a model in which the panel is regularly ribbed so that situations in which the equality in the separations between adjacent ribs is disturbed cannot be investigated with $\overline{B}_s^I(k)$. (To investigate how the influence of fluid loading is coupled to variations in the separations between ribs, one needs to switch from Eq. (21) to Eq. (18). Such considerations, however, lie outside the scope of this paper.) Since the factor B_0^I is independent of k, the quantity $\overline{B}_s^I(k)$ is aliased and symmetric in k in the manner specified for $B_s^I(k)$ in Eq. (53). Figure 15 is intended to illustrate the invariance of these properties to changes in the parameters that describe the regularly ribbed fluid loaded panel. Indirectly, but clearly, the influence of the same changes on the phenomenon of the pass and stop bands is also illustrated in this figure.[4] The magnitudes of $\overline{B}_s^I(k)$ as functions of the normalized wavenumber (k/κ_1) for discrete, successive, and equal increments of the normalized frequency (ω_1/ω_c) are displayed in Fig. 15. In

Fig. 15 the threshold t^0 is conveniently chosen to be 1.5. [cf. Fig. 4d.] In Fig. 15a, the standard conditions are maintained. In Fig. 15b the fluid loading parameter ϵ_c is changed from its standard value of 0.1 to the much lower value of 0.001. Although the phenomenon of pass and stop bands is manifested more distinctly in Fig. 15b than in Fig. 15a, it is still amply evident in the latter figure. Figures 15c and d depict situations which correspond to those depicted in Figs. 15a and b, respectively, except that the standard value of the surface mass ratio (M/bm) is changed from its standard value of 0.3 to the high value of $3x10^3$; in this case, the magnitude of the line impedance Z^I of the ribs exceeds by far the magnitude of the line impedance g^I_∞ of the uniform panel. Even in this extreme case, the pass and stop bands are evidenced and, again, the fluid loading does not substantially suppress this phenomenon. Figures 15a and b are repeated in Figs. 15e and f for situations in which the separation b between adjacent ribs is decreased so that $bk_c = 4$ and the mass per unit length of the ribs is proportionately decreased so that (M/bm) is maintained at its standard value of 0.3. The phenomenon of pass and stop bands is present in Figs. 15d and e, in a similar fashion to its presence in Figs. 15a and b, respectively. The aliasing and the symmetry of $B^I_s(k)$ in k are evidenced throughout Fig. 15, thus confirming the invariance of these properties in this factor to changes in the parameters that describe a regularly ribbed fluid loaded panel. Finally, the invariance of aliasing in $B^I_s(k)$ in k indicates that the introduction of fluid loading does not cause biases in the k-domain in favor or disfavor of low and high wavenumber distributions. Thus, one may conclude that the interactions among the ribs cannot be made to distinguish between low and high wavenumber components in the k-domain. [cf. Appendix A.]

REFLECTION COEFFICIENT IN THE FAR-FIELD

The reflection coefficients defined in the preceeding sections are related to the pressure waves perceived on a plane that is placed on the surface of the panel. One may ask for the corresponding reflection coefficients were one to assess the reflected pressure waves on a control-semi-cylindrical surface in the far-field. The far-field reflected pressure wave due to the collimated

incident pressure wave specified in Eq. (37), say, is given by

$$p_x^I(r,\theta) = P_{I0}\,\Gamma_x^I(\theta)\,(\pi/2)^{1/2}\,H_0^{(2)}\,[(Y_f^I\omega_I/c)\,r]\;;$$
$$r = (x^2 + z^2)^{1/2}\;;\quad (\omega_I r/c) >> 1\;, \tag{55}$$

where $H_0^{(2)}$ is the Hankel function of the second kind and of order zero [6]. Explicitly, the factors $\Gamma_x^I(\theta)$ and Y_f^I are of the forms

$$\Gamma_x^I(\theta) = Y_f^I\cos(\theta)\,R_x^I(\kappa^I \mid k_I)\;;\quad \kappa^I = (Y_f^I\,\omega_I/c)\,\sin(\theta)\;, \tag{56}$$

$$Y_f^I = [1 - (k_{yI}c/\omega_I)^2]^{1/2}\;;\quad (k_{yI}c/\omega_I)^2 < 1\;, \tag{57}$$

and $R_x^I(k \mid k_I)$ is as stated in Eq. (38). The quantity $\Gamma_x^I(\theta)$ is limited to the supersonic components in $R_x^I(k \mid k_I)$ only. The subsonic components do not reach the far-field; they are filtered out by the passage through the fluid from the surface of the panel to the far-field locations. The far-field reflection coefficient $\bar{\Gamma}_x(\theta)$ is defined

$$\bar{\Gamma}_x(\theta) = (2\pi/L_x)\,\Gamma_x^I(\theta)\;. \tag{58}$$

[cf. Eq. (39).] This quantity is, in fact, merely a directivity factor describing the directivity of the reflected pressure waves in the far-field. [$\bar{\Gamma}_x(\theta)$ is related generically to the reflection "form-function" in cylindrical geometry [8].] The regularly ribbed fluid loaded panel is chosen as a computational example. Accordingly Eqs. (43) through (46) are substituted in Eqs. (56) to obtain

$$\bar{\Gamma}_x^I(\theta) = \bar{\Gamma}_{0x}^I(\theta) + \bar{\Gamma}_{sx}^I(\theta)\;, \tag{59}$$

$$\bar{\Gamma}_{0x}^I(\theta) = Y_f^I\cos(\theta)\,[1 - 2\Lambda_\infty^I(\kappa^I)]\,\bar{F}_x(\kappa^I - k_I)\;, \tag{60}$$

$$\bar{\Gamma}^{I}_{sx}(\theta) = Y^{I}_{f}\cos(\theta)\,\Lambda^{I}(\kappa^{I})\,\bar{\bar{R}}_{sx}(\kappa^{I} \mid k_{I}) \quad , \tag{61}$$

where $\bar{\bar{R}}^{I}_{sx}(k \mid k_{I})$ is defined in Eq. (46) and it is noted that

$$\Lambda^{I}_{\infty}(\kappa^{I}) = \left[\{Z^{I}_{p}(\kappa^{I})/\rho c\}\, Y^{I}_{f}\cos(\theta) + 1\right]^{-1} \quad , \tag{62}$$

where $Z_p(k)$ is defined and stated in Eqs. (16) and (17). The magnitude of $\bar{\Gamma}^{I}_{x}(\theta)$, as stated in Eqs. (59) through (61), is displayed as a function of θ in Fig. 16. In Figs. 16a, b, and c the normalized frequency (ω_I/ω_c) is set at 0.25, 0.4, and 0.5, respectively, the standard conditions are imposed, and the first order model is assumed; i.e., $\bar{\bar{R}}^{I}_{sx}(k \mid k_{I})$ in these figures is expressed in Eq. (46b). In Figs. 16d, e, and f the respective normalized frequencies and standard conditions are imposed, however and notably, the proper model is assumed; i.e., $\bar{\bar{R}}^{I}_{sx}(k \mid k_{I})$ in these figures is expressed in Eq. (46a). The normalized frequency (ω_I/ω_c) = 0.25 is chosen so that the first negative diffraction order coincides approximately with a monostatic return, and the normalized frequency (ω_I/ω_c) = 0.5 is chosen so that the second negative diffraction order coincides approximately with a monostatic return. [In the latter case the first negative diffraction order coincides approximately with a normal return, see Figs. 16c and f.] The differences between the figures in the three pairs: Figs. 16a and d; Figs. 16b and e; and Figs. 16c and f, can be attributed to the phenomenon of pass and stop bands. This phenomenon influences significantly the highlights in the results reported in Figs. 16d, e, and f. Features of significance in Figs. 16a, b, and c are largely modified, and are even absent, in Figs. 16d, e, and f. [cf. Figs. 8b and a.] Thus, when structural regularities are present in a structure, the reflection of pressure waves by the structure to the far-field may depend critically on the existence and disposition of the phenomenon of pass and stop bands. Since the pass and stop bands phenomenon is sensitive to various parameters that

describe the structure and its environmental loading, the determination of the highlights in the reflection from such a structure cannot be cavalierly approximated.

Figure 16g repeats Fig. 16e except that the fluid loading parameter ε_c is changed from the standard value of 0.1 to 0.001. By comparing these figures and consulting previous figures, e.g., Figs.8b, 10b, and 13b, it is clear that in Fig. 16g the contribution to the far-field reflection coefficient $\overline{\Gamma}^I_x(\theta)$ by the term $\overline{\Gamma}^I_{0x}(\theta)$ is overriding. This statement is made clear by presenting Fig. 16h, in which the term $\overline{\Gamma}^I_{sx}(\theta)$ only is displayed. Thus, when structural regularities are present in a structure, the reflection of pressure waves by the structure to the far-field may not necessarily exhibit a dependence on the phenomenon of pass and stop bands; other diffraction mechanism may be dominant. Even in this simplified model of the structure it appears that multiplicity of angular variations occur in the reflection and that these variations are sensitive to parameters that describe the structural form, e.g., apertures in the structure and in the incident pressure wave.

APPENDIX A

There are some advantages in investigating the nature of the factor $\overline{B}_s(k, \omega_2)$ in the spatial domain. If one denotes by $g_{1s}(x \mid x', \omega_2)$ the impulse response function for a first order model of a regularly ribbed fluid loaded panel and the corresponding impulse response function for a proper model by $g_s(x \mid x', \omega_2)$,then by definition

$$g_s(x \mid x', \omega_2) = \int \overline{b}_s(x - x'', \omega_2)\ dx''\, g_{1s}(x'' \mid x', \omega_2) \quad , \tag{A1}$$

where [1]

$$\overline{b}_s(x, \omega_2) = (2\pi)^{-1/2} \int \overline{B}_s(k, \omega_2)\ dk\ \exp(-ikx) \quad , \tag{A2}$$

$$g_s(x \mid x', \omega_2) = (2\pi)^{-1} \int G_s(k \mid k', \omega_2)\ dx\, dx' \exp[i(xk - x'k')] \quad , \tag{A3}$$

Using the aliasing and symmetry properties of $\overline{B}_s(k, \omega_2)$ in k, one may state Eq. (A2) in the form

$$\overline{b}_s(x, \omega_2) = (2\pi)^{1/2} \sum_j \overline{\overline{b}}_s(x_j, \omega_2)\ \delta(x - x_j) \quad ; \quad \overline{\overline{b}}_s(x_j, \omega_2) = \overline{\overline{b}}_s(-x_j, \omega_2) \quad , \tag{A4}$$

where

$$\overline{\overline{b}}_s(x_j, \omega_2) = (\kappa_1)^{-1} \int_0^{\kappa_1} \overline{B}_s(k, \omega_2)\ dk \exp(-ikx_j) \quad . \tag{A5}$$

It is recalled that the aliasing and symmetry of $\overline{B}_s(k, \omega_2)$ in k is invariant to reasonable changes in the parameters that describe the regularly ribbed fluid loaded panel and, therefore, Eqs. (A4) and (A5) are similarly invariant. A Fourier transformation of Eq. (A4) yields

$$\bar{B}_s(k, \omega_2) = \sum_j \bar{\bar{b}}_s(x_j, \omega_2) \exp(ikx_j) \quad , \tag{A6}$$

Thus, $\bar{\bar{b}}_s(x_j, \omega_2)$ is the (j)th coefficient in the Fourier series expansion of $\bar{B}_s(k, \omega_2)$ with respect to k. For the records, it may be noted that

$$\sum_j \tilde{H}_\infty(k + \kappa_j, \omega_2) = \bar{g}_0(\omega_2) \sum_j \bar{g}_\infty(x_j, \omega_2) \exp(ikx_j) \quad . \tag{A7}$$

From Eqs. (A1) and (A4), one obtains

$$g_s(x \mid x', \omega_2) = \sum_j \bar{\bar{b}}_s(x_j, \omega_2)\, g_{1s}(x - x_j \mid x', \omega_2) \quad . \tag{A8}$$

A Fourier transformation of Eq. (A8) yields

$$G_s(k \mid k', \omega_2) = \bar{B}_s(k, \omega_2)\, G_{1s}(k \mid k', \omega_2) \quad , \tag{A9}$$

where use is made of Eq. (A6). The factorial relationship in Eq. (A9) between G_s and G_{1s} in the k-domain is convenient, as the material in the text made clear. [cf. Eqs. (21) and (46).] Can one obtain a similar factorial relationship between g_s and g_{1s} in the x-domain? One may, in this vein, construct from Eq. (A8) the form

$$g_s(x \mid x', \omega_2) = [\, \bar{\bar{b}}_s(0, \omega_2) + \gamma_s(x \mid x', \omega_2)]\; g_{1s}(x \mid x', \omega_2) \quad . \tag{A10}$$

where

$$\gamma_s(x \mid x', \omega_2) = \sum_{j \neq 0} \bar{\bar{b}}_s(x_j, \omega_2)\, \{g_{1s}(x - x_j \mid x', \omega_2) / g_{1s}(x \mid x', \omega_2)\} \quad , \tag{A11}$$

It is apparent that Eq. (A10) is not as elegant and straightforward as Eq. (A9) is. However, it is asserted that the term $\bar{\bar{b}}_s(0, \omega_2)$ is a significant term in the bracketed factor in Eq. (A10) and, therefore, its behavior is significant to the relationship expressed in Eq. (A10). At least Eq. (A10) is more compact than is the equation obtained directly by a Fourier transformation of Eq. (18). The magnitude of the zeroth coefficient $\bar{\bar{b}}_s^I(0)$ as a function of the normalized frequency (ω_I/ω_c) under standard conditions is computed and displayed in Fig. A1. In Fig. A2 the fluid loading parameter ε_c is changed from its standard value of 0.1 to 0.001. The pass and stop bands phenomenon is made apparent in this zeroth coefficient. It is also apparent that increase in fluid loading tends to dull this phenomenon. The investigation here proposed remains incomplete without some examination of the behavior of γ_s in Eqs. (A10) and (A11). However, this examination lies outside the scope of the paper in which Eq. (A9), rather than Eq. (A8), is basic. In this sense, Fig. A, displaying $\bar{\bar{b}}_s^I(0)$, may be viewed as the integrated measure of Fig. 15, displaying $\bar{B}_s^I(k)$.

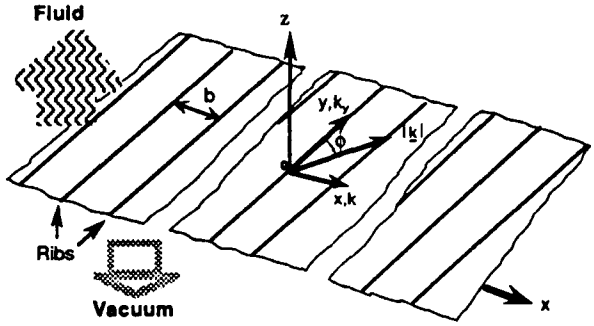

Fig. 1. A sketch of a ribbed fluid loaded panel showing the coordinate system and the orientation of the ribs.

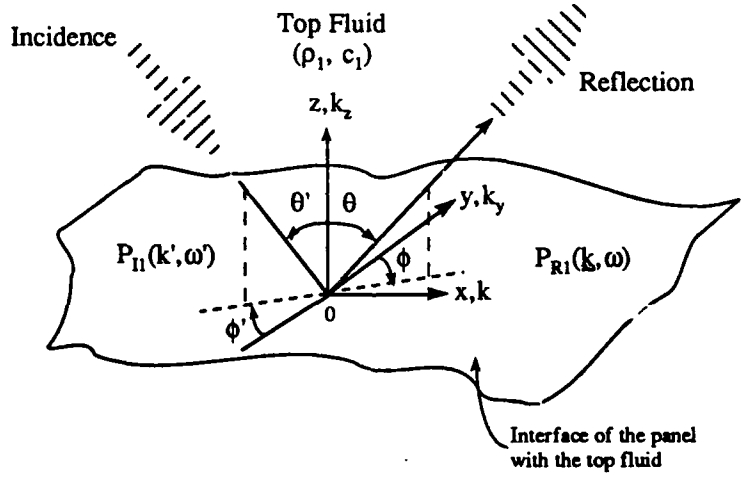

Fig. 2. Incident pressure $P_{I1}(k',\omega')$ and reflected pressure $P_{R1}(k,\omega)$ on the interface between the top fluid and the panel.

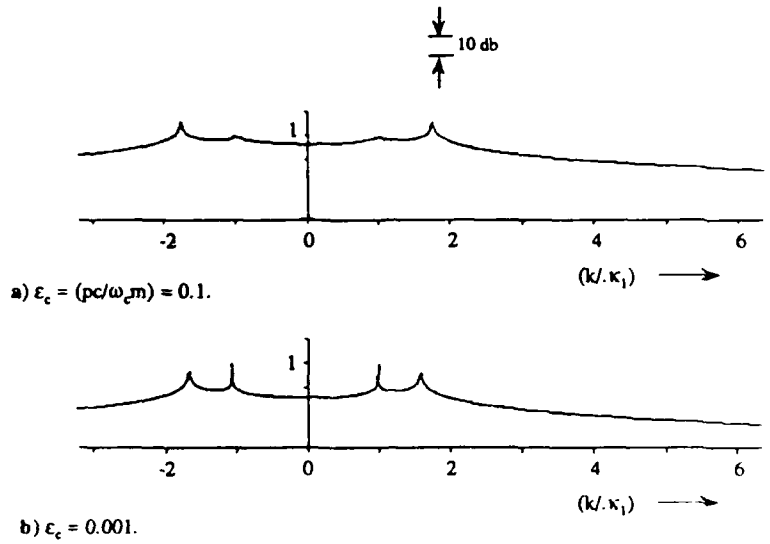

Fig. 3. The magnitude of the factor $\Lambda^{I}_{-}(k)$ [Eq. (41)] as a function of the normalized wavenumber (k/κ_1) at the fixed normalized frequency $(\omega_f/\omega_c) = 0.4$ with $\phi_I = 0$. The panel is an isotropic membrane that simulates a plate responding in flexure. The free wavenumber $k_p = (\omega_f\omega_c/c^2)^{1/2}(1 + i\eta_p)$ and the loss factor η_p is chosen equal to 0.005.

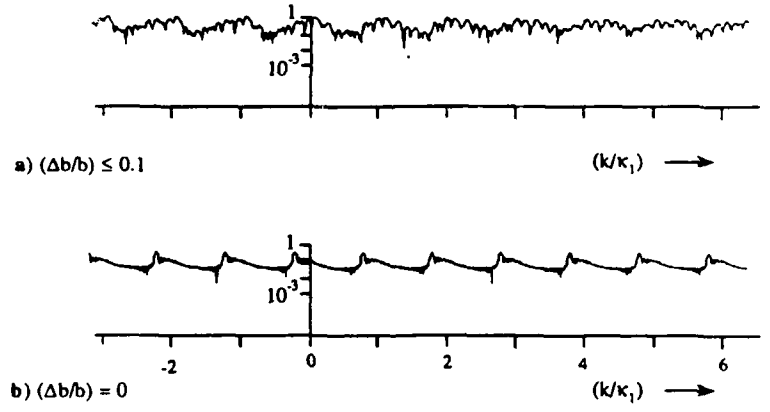

Fig. 5. The magnitude of the factor $\bar{\bar{R}}^{1}_{e}(k|k_i)$ [Eq. (42a)] in the reflection coefficient due to the ribs as a function of the normalized wavenumber (k/κ_1) at the fixed normalized frequency $(\omega_f/\omega_c) = 0.4$ with $\theta_I = 0.9$ and $\phi_I = 0.0$. Incident pressure wave is a plane wave. The panel is as in Fig. 3a. The line impedance of the ribs is mass controlled $Z_j = Z = i\omega M$, with $(M/bm) = 0.3$, $\varepsilon_c = 0.1$, and $(b\omega_c/c) = 16$, where m is the mass per unit area of the panel and b is a typical separation between adjacent ribs. A typical deviation in b is designated by Δb. The array consists of 21 ribs.

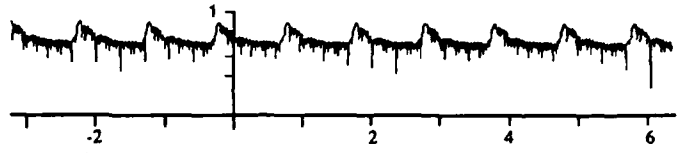

a) The factor $|\bar{\bar{R}}^I_{xx}|$ in the proper model with $\theta_I = 0.9$.

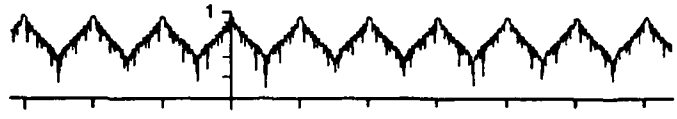

b) The factor $|\bar{\bar{R}}^I_{xx}|$ in the proper model with $\theta_I = 0.0$.

b) The factor $|\bar{\bar{R}}^I_{xx}|$ in first order model with $\theta_I = 0.9$.

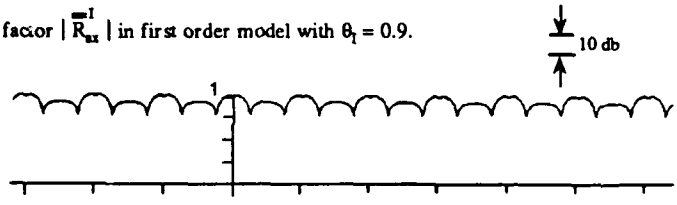

d) The factor $|B^I_s(k)|$ [Eqn. 47a] as a function of the normalized wavenumber (k/κ_1) for the conditions used in Fig. 4a.

Fig.4 The magnitudes of $\bar{\bar{R}}^I_{xx}$ and the factor B^I_s [Eq. (46a)] in the reflection coefficient due to the ribs as a function of the normalized wavenumber (k/κ_1) at the normalized frequency $(\omega_p/\omega_c) = 0.4$ with $\phi_1 = 0$. The incident pressure wave is collimated with an aperture of 21 ribs. The panel is as in Fig. 3a. The line impedances of the ribs are mass controlled, $Z_j = Z = i\omega M$, with $(M/bm) = 0.3$, and $(b\omega_c/c) = 16$, where m is the mass per unit area of the panel and b is a typical separation between ribs.

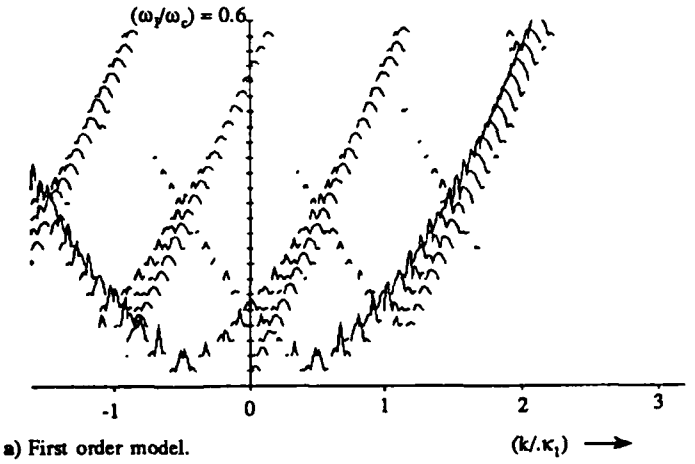

a) First order model.

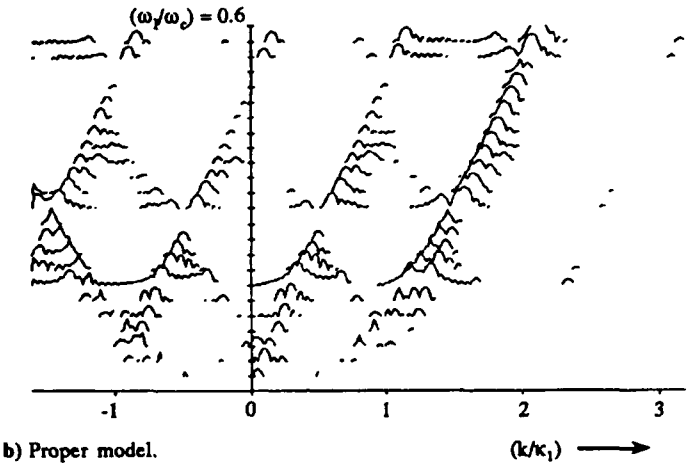

b) Proper model.

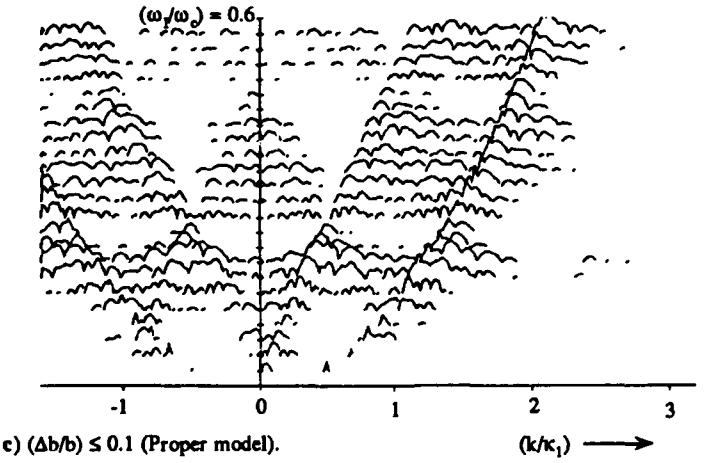

c) $(\Delta b/b) \leq 0.1$ (Proper model).

Fig. 6. Magnitude of the reflection coefficient $\overline{R}_s^I(k|k_1)$ due to the ribs [Eq. (42)] as a function of the normalized wavenumber (k/κ_1) in the standard format and under standard conditions.

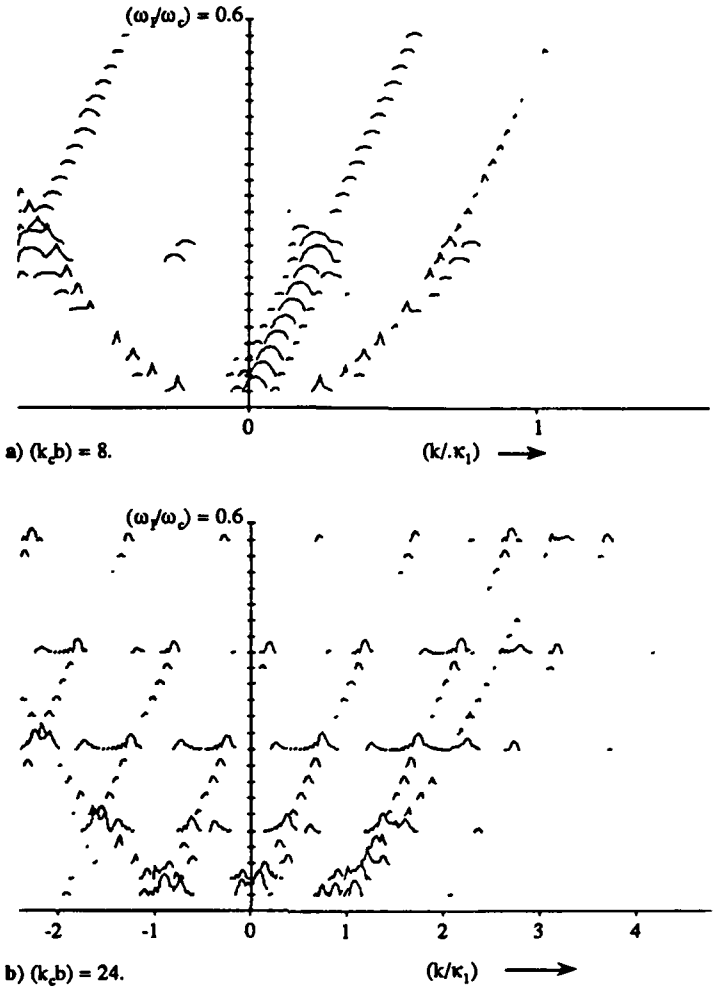

Fig. 7. Magnitude of the reflection coefficient $\overline{R}_s^I(k|k_1)$ for the proper model [Eq. (42a)] as a function of the normalized wavenumber (k/κ_1) in the standard format and under standard conditions with the exception that instead of the standard value of $(k_c b) = 16$, the value is as noted.

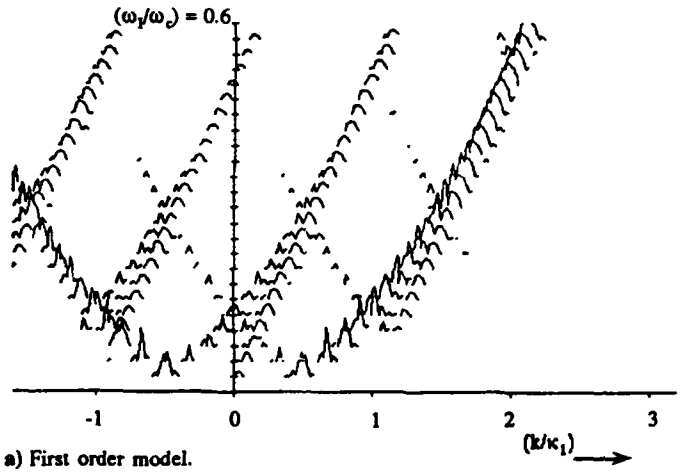

a) First order model.

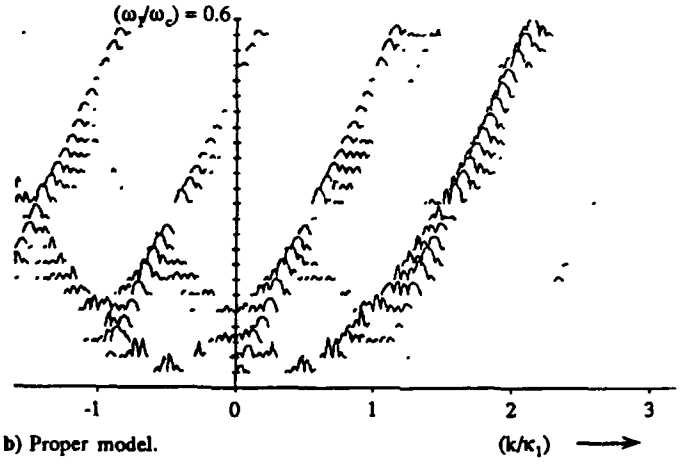

b) Proper model.

Fig. 8. Magnitude of the reflection coefficient $\bar{R}^I_{xx}(k|k_1)$ due to ribs [Eq.(46)] as a function of the normalized wavenumber (k/κ_1) in the standard format and under standard conditions.

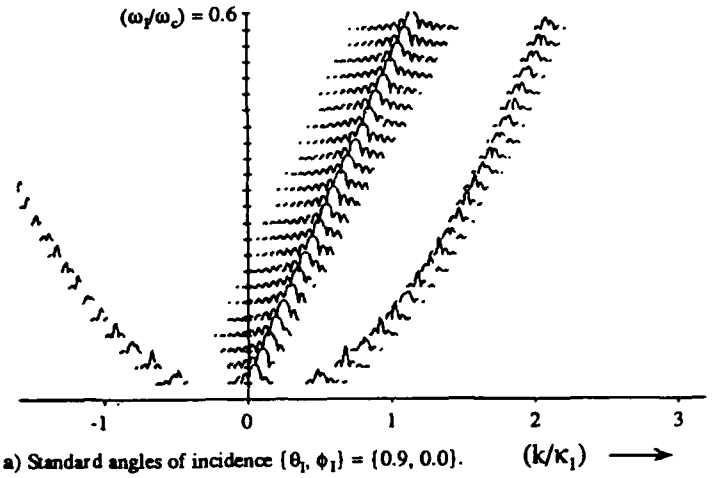

a) Standard angles of incidence $\{\theta_1, \phi_1\} = \{0.9, 0.0\}$.

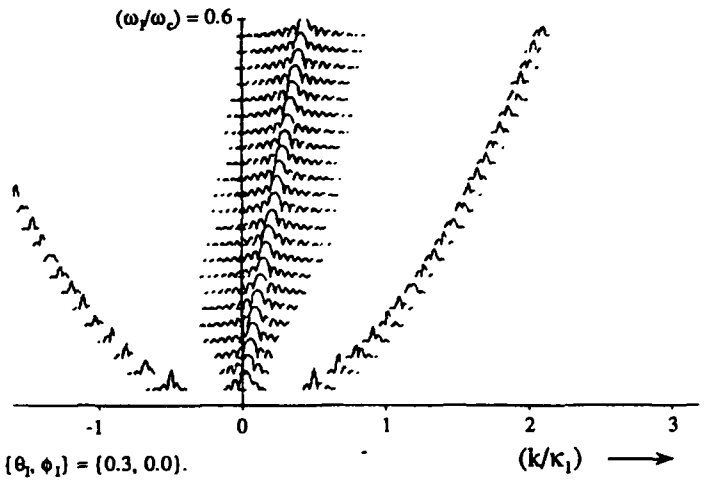

b) $\{\theta_1, \phi_1\} = \{0.3, 0.0\}$.

Fig.9. Magnitude of the reflection coefficient $\overline{R}^{I}_{0\alpha}(k|k_1)$ in the absence of ribs [Eq. (42)] as a function of the normalized wavenumber (k/κ_1) in the standard format and under standard conditions for the panel except for the angles of incidence as noted.

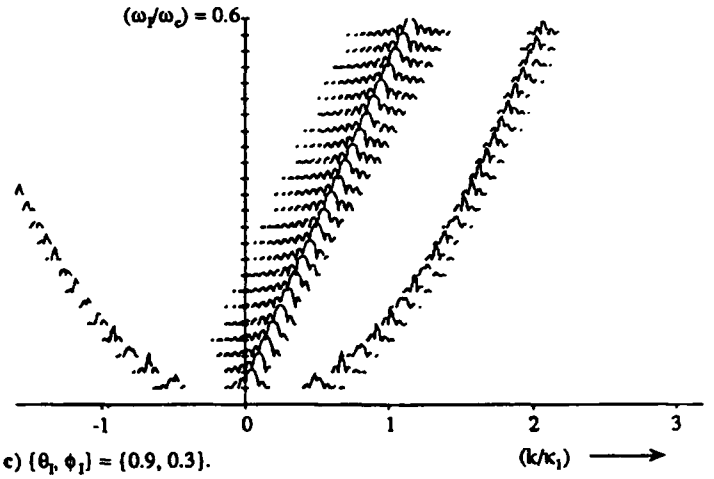

c) $\{\theta_1, \phi_1\} = \{0.9, 0.3\}$.

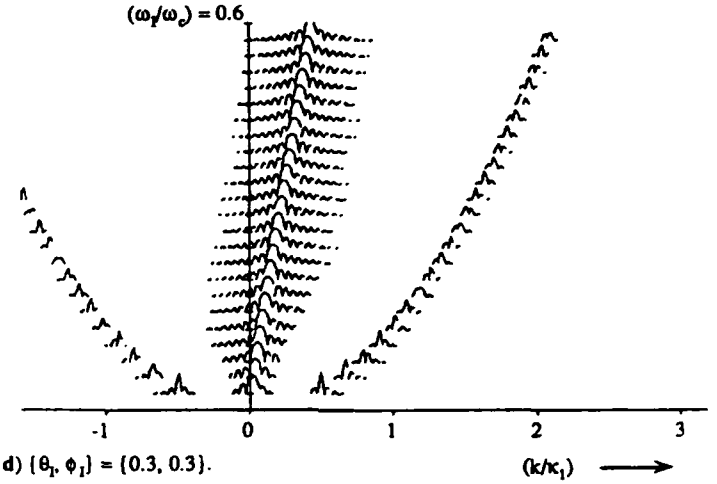

d) $\{\theta_1, \phi_1\} = \{0.3, 0.3\}$.

Fig. 9 continued.

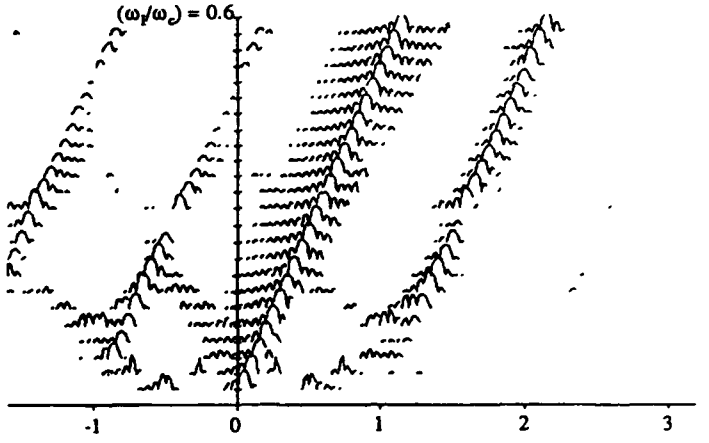

a) Standard angles of incidence $\{\theta_1, \phi_1\} = \{0.9, 0.0\}$.

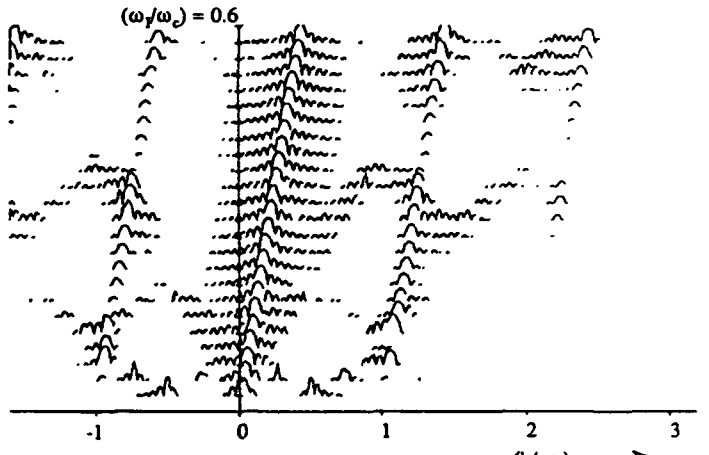

b) $\{\theta_1, \phi_1\} = \{0.3, 0.0\}$.

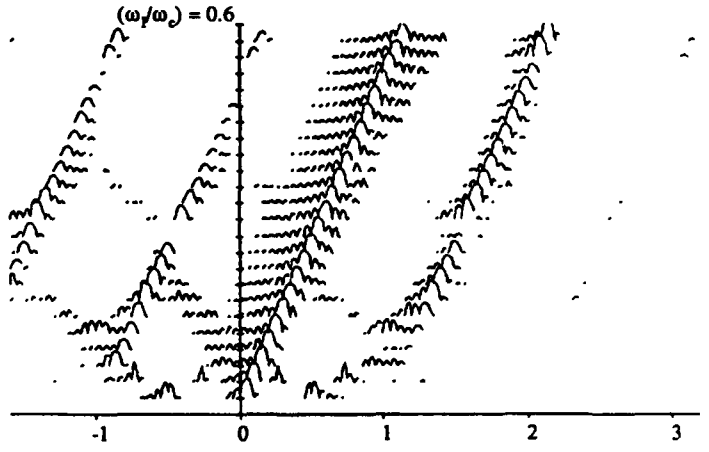

c) $\{\theta_1, \phi_1\} = \{0.9, 0.3\}$.

Fig. 10. Magnitude of the reflection coefficient $\bar{R}_z^I(k|k_1)$ [Eq.(43)] as a function of the normalized wavenumber (k/κ_1) in the standard format and under standard conditions except for the angle of incidence as noted.

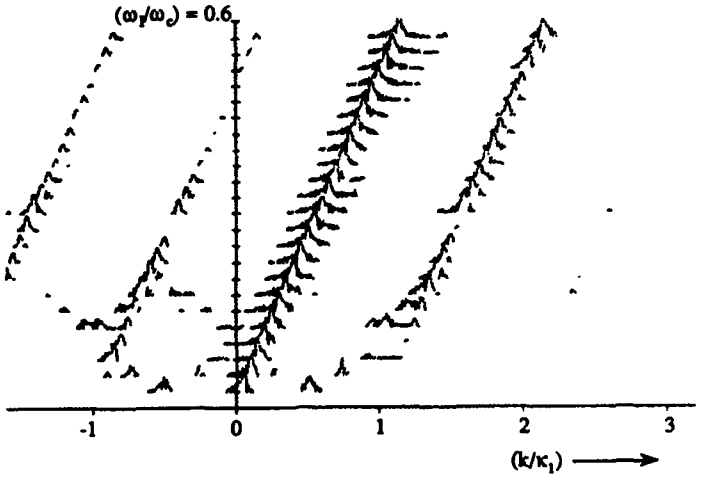

Fig. 11. Repeats Fig.10a with a change in the aperture from the standard value of 20b (21 ribs) to 42b (41 ribs).

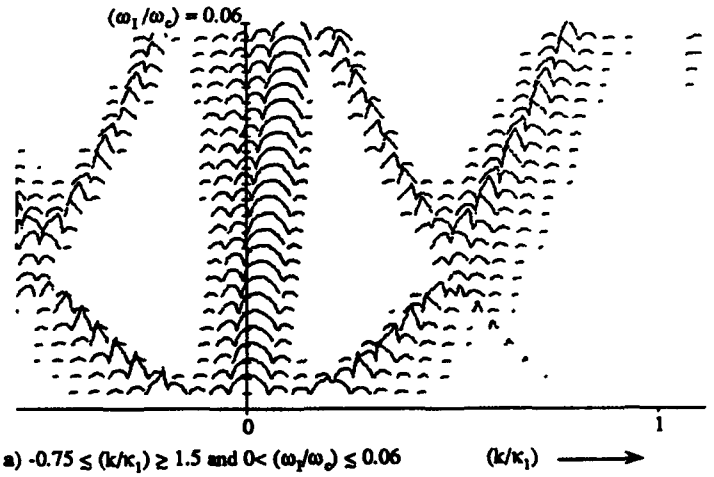

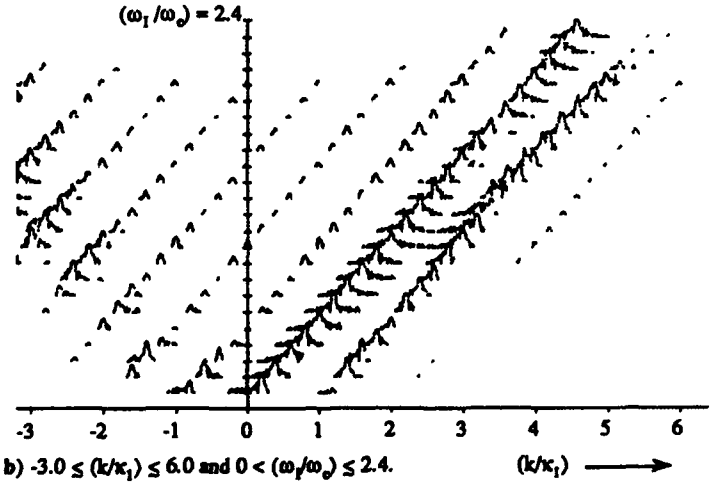

Fig. 12. Repeats Fig.10a with a change in the wavenumber-frequency range displayed from the standard range $-1.5 \leq (k/\kappa_1) \leq 3.0$ and $0 < (\omega_I/\omega_o) \leq 0.6$ to the values noted.

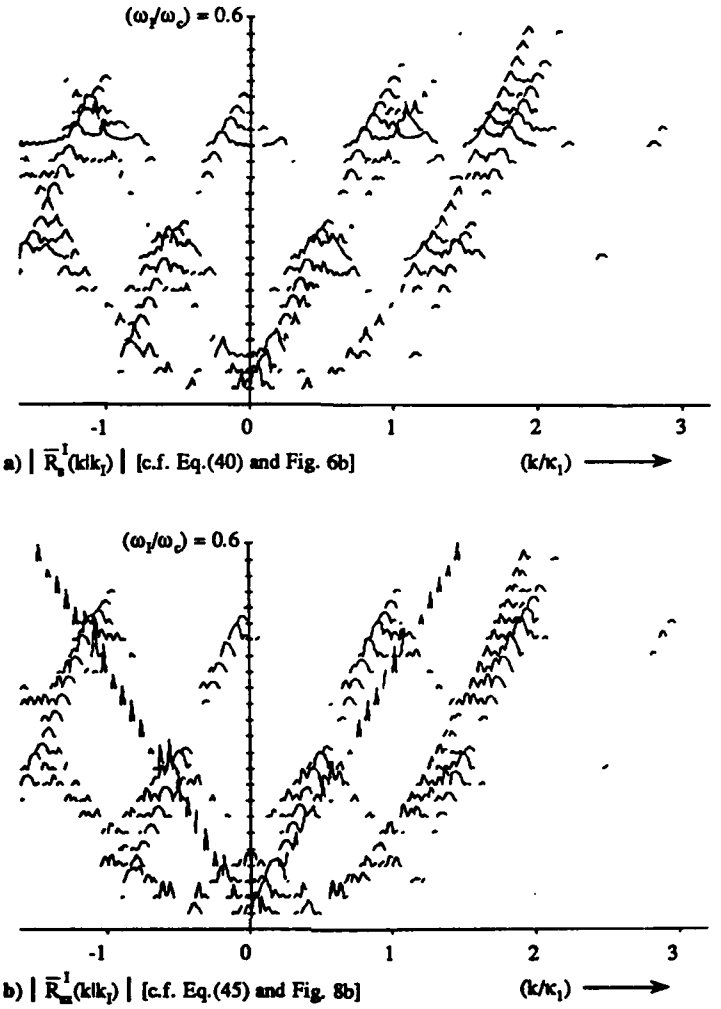

Fig. 13. Magnitude of the reflection coefficient except that the value for the fluid loading parameter, ε_c, and the threshold, t^0, are changed from their standard values of 0.1 and 0.03, respectively, to 0.001 and 0.001, respectively.

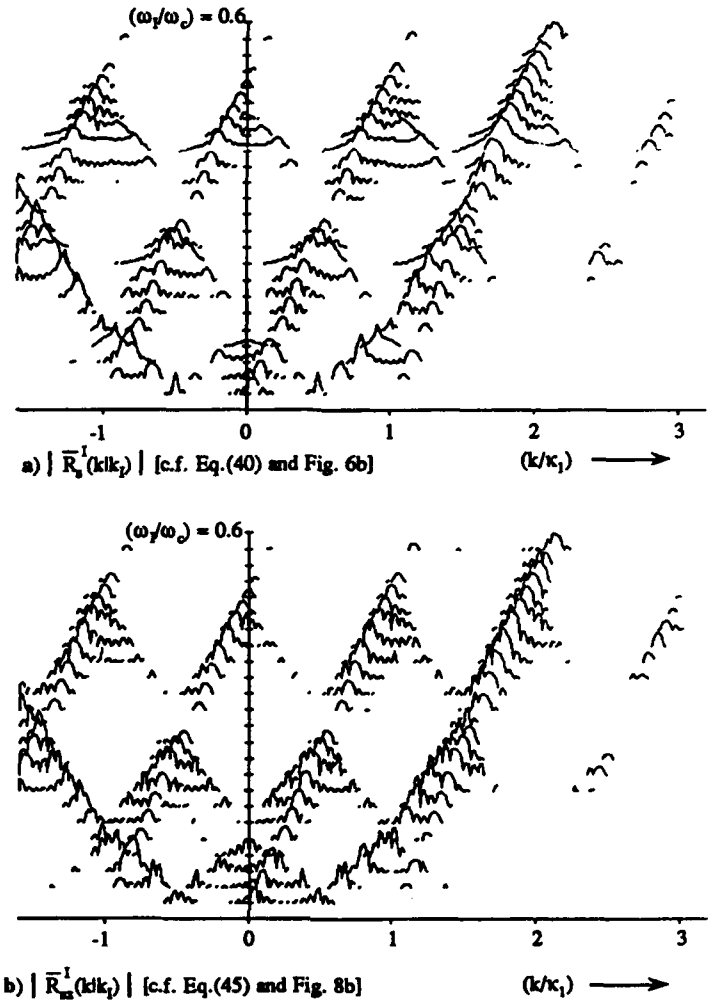

Fig. 14. Magnitude of the reflection coefficient where the fluid loading is partially accounted for; namely only in the factor $\Lambda_m^I(k)$.

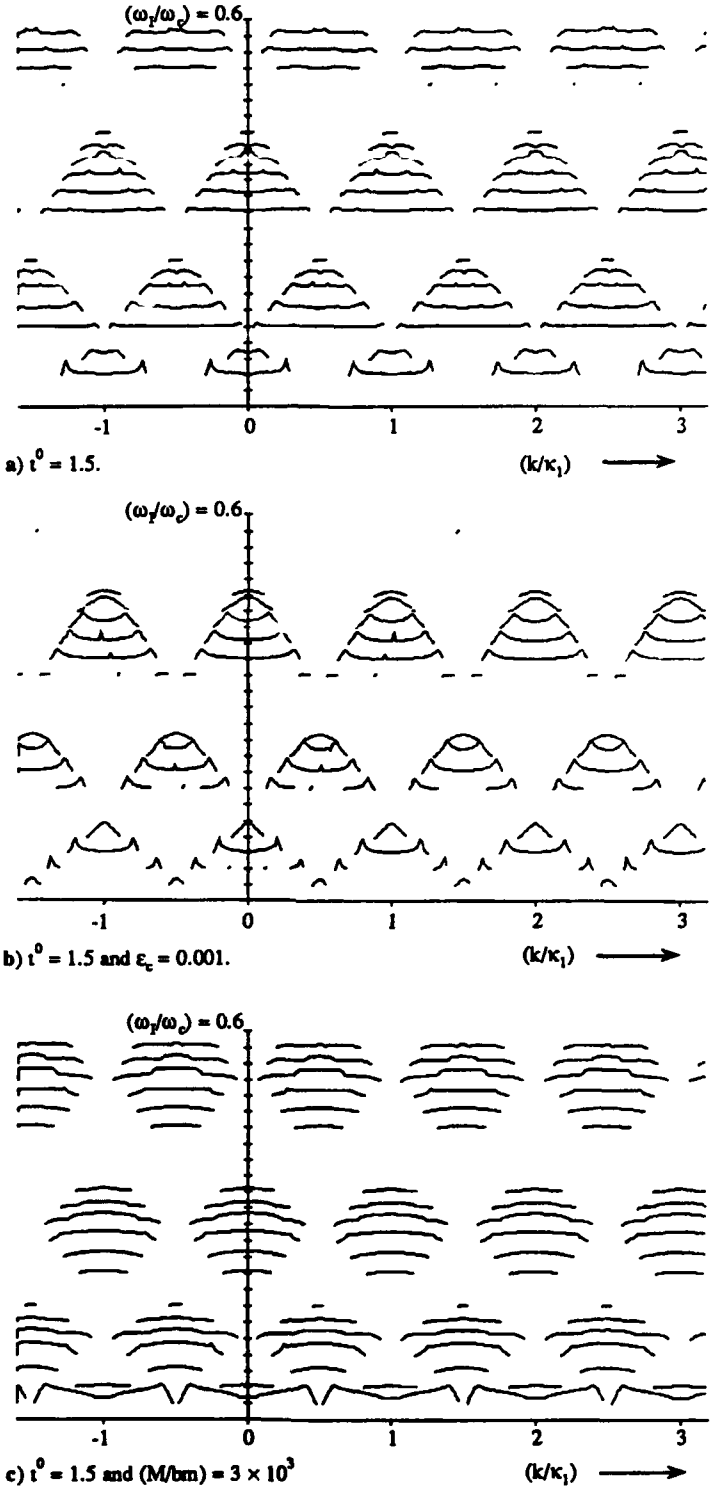

Fig.15 The. Magnitude of the interaction factor $\overline{B}_s^I(k)$ as a function of the normalized wavenumber (k/κ_1) in the standard format. The standard conditions are maintained except as noted.

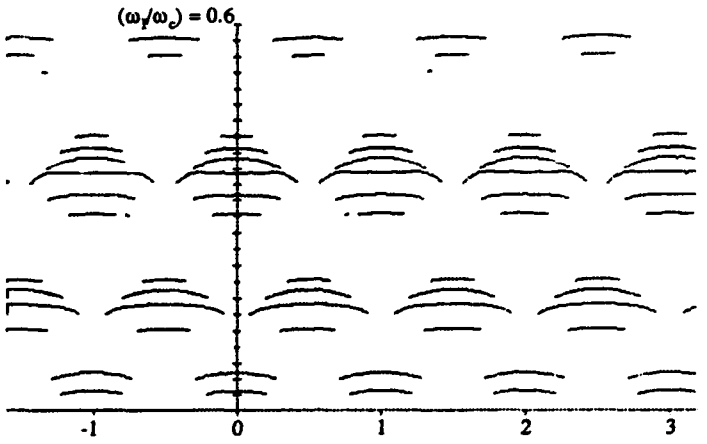

d) $t^0 = 1.5$, $(M/bm) = 3 \times 10^3$, and $\varepsilon_c = 0.001$.

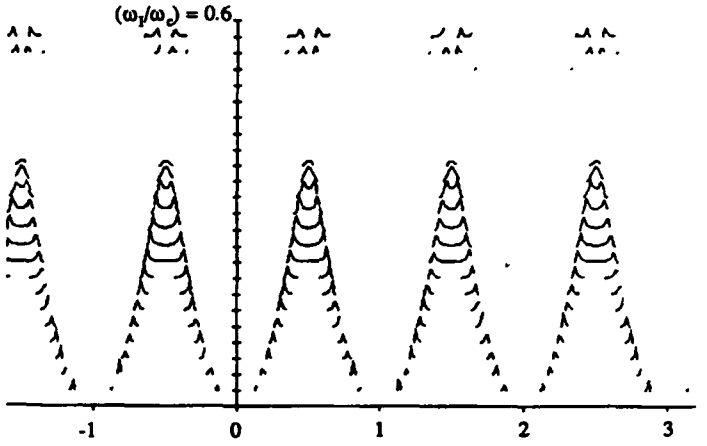

e) $t^0 = 1.5$, and $bk_c = 4$.

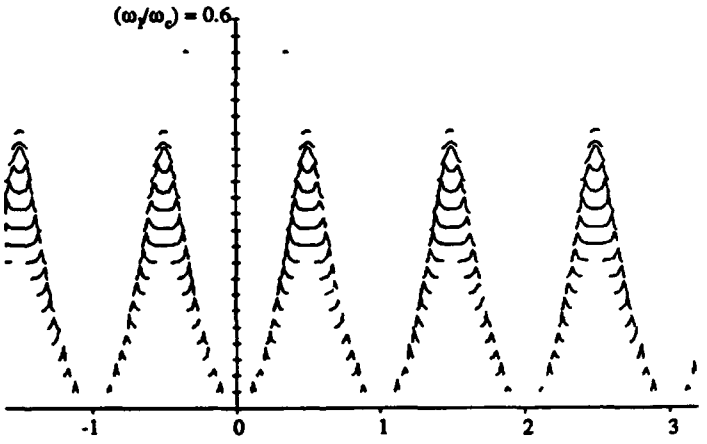

f) $t^0 = 1.5$, $\varepsilon_c = 0.001$, and $bk_c = 4$.

Fig. 15. Continued.

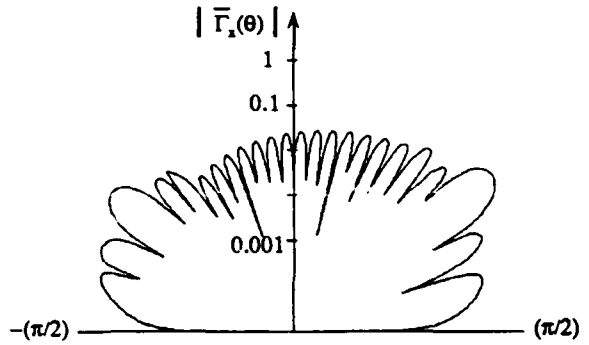

a) First order model and $(\omega_1/\omega_c) = 0.25$.

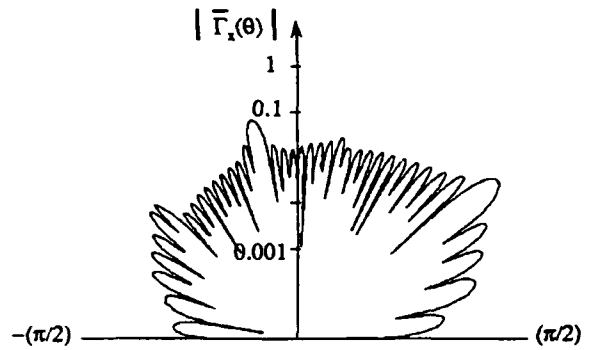

b) First order model and $(\omega_1/\omega_c) = 0.4$.

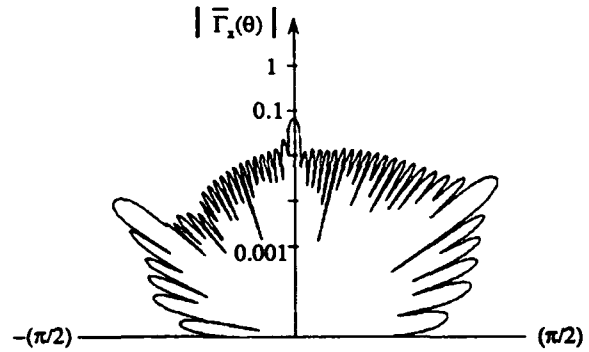

c) First order model and $(\omega_1/\omega_c) = 0.5$.

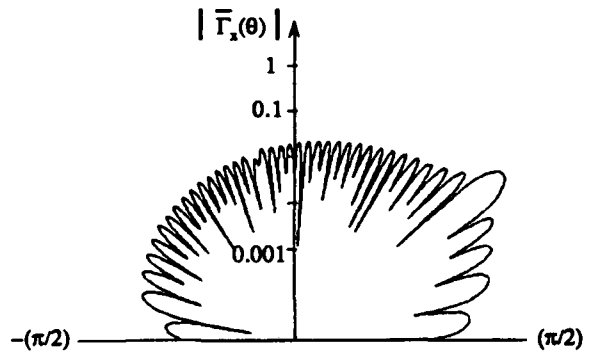

g) Repeats Fig. 16e except that the fluid loading parameter ε_c is changed from its standard value of 0.1 to 0.001.

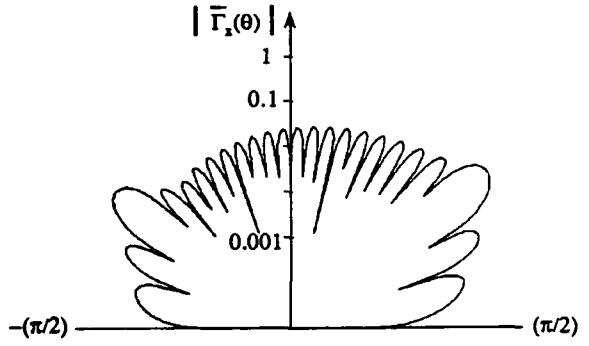

d) Proper order model and $(\omega_1/\omega_c) = 0.25$.

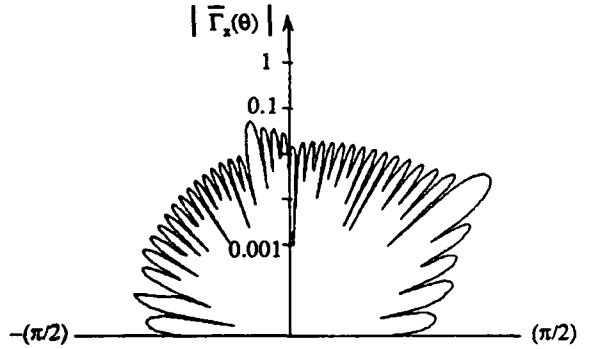

e) Proper order model and $(\omega_1/\omega_c) = 0.4$.

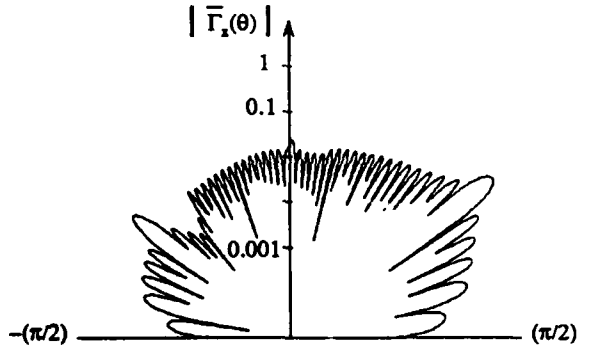

f) Proper order model and $(\omega_1/\omega_c) = 0.5$.

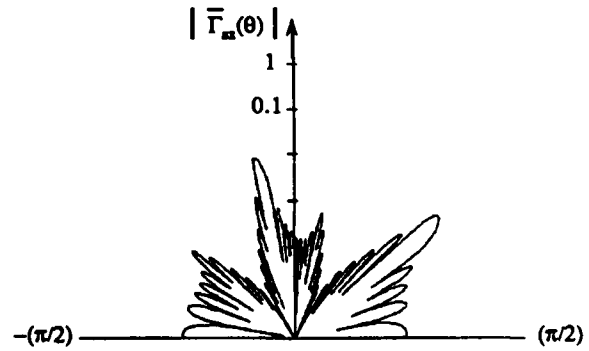

h) The magnitude of the far-field reflection coefficient due to ribs under standard conditions except fluid loading as in Fig. 16g.

Fig. 16. The magnitude of the far-field reflection coefficient in a polar plot with respect to the angle (θ).

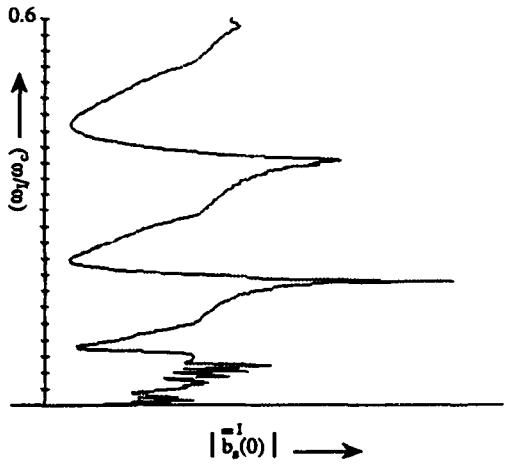

Fig. A1 The magnitude of the Fourier series coefficient $\bar{b}_0^{-1}(0)$ [Eqs. (A4), (A5) and (A10)] as a function of the normalized frequency (ω_f/ω_c) under standard conditions.

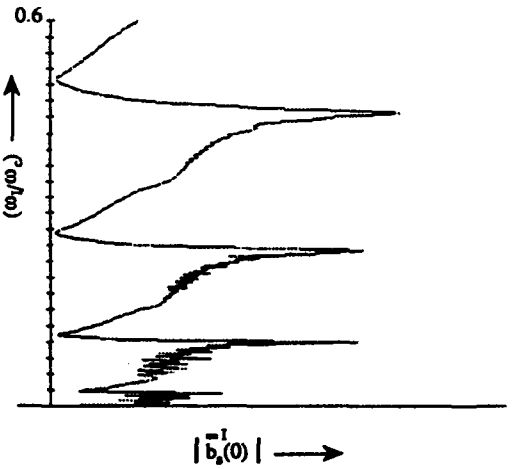

Fig. A2 Repeats Fig. A1 except that the fluid loading parameter ε_c is changed from the standard value of 0.1 to 0.001.

REFERENCES

1. G. Maidanik and J. Dickey 1988 *Journal of Sound and Vibration* 123, 293-307. Acoustic behavior of ribbed panels.

2. G. Maidanik and J. Dickey 1989 *Journal of Sound and Vibration* 000, 000-000. Velocity distribution on unloaded finitely and regularly ribbed membranes.

3. G. Maidanik and J. Dickey 1991 *Journal of Sound and Vibration* 000, 000-000. Response of regularly ribbed fluid loaded panels.

4. G. Maidanik and A. J. Tucker 1976 *Journal of Sound and Vibration* 44, 267-274. Proper and first order solutions of regularly ribbed panels.

5. G. Maidanik and J. Dickey 1991 *Acustica* 000, 000-000 . Localization and delocalization.

6. G. Maidanik, J. Dickey and J. Ertel 1989 *Journal of Sound and Vibration* 000, 000-000. Partial radiation efficiency of line driven panels.

7. G. Maidanik and J. Dickey 1990 Submitted for publication in the Journal of Sound and Vibration. Aliasing in the response of ribbed panels.

8. W. G. Neubauer (1976-1980) Acoustic reflection from surfaces and shapes (Naval Research Laboratory, Washington, D.C.)

INITIAL DISTRIBUTION

Copies		Copies	
2	ONT (Remmers)	1	1905.3 (Feit)
3	ONR	1	1906 (Vendettis)
	121 (Hansen)	1	1908 (McKeon)
	11 (Reischmann)	1	192
	1132SM (Abraham)	1	1921 (King)
3	NAVSEA	1	1926 (Keech)
	2 SEA 55N (Biancardi)	1	193
	1 SEA 92R	1	194
1	DARPA	1	1942 (Hwang)
12	DTIC	1	1944 (Maga)
2	USNA Physics Depart. (Ertel)	1	1965 (Niemiec)
	CENTER DISTRIBUTION	1	27
1	01A	1	2704
1	0112 (Halsall)	10	2704.1
1	0113	1	274
		1	2741
1	17	1	2742
1	172	1	2743
		1	2744
1	18	1	2749
1	19	1	284
1	1902		
1	1903 (Smith)	1	342.1 TIC(C)
1	1905.1 (Blake)	1	342.2 TIC(A)
		2	3431
		10	3432 Reports Control

REPORT DOCUMENTATION PAGE

Form Approved
OMB No. 0704-0188

1. AGENCY USE ONLY *(Leave blank)*	2. REPORT DATE	3. REPORT TYPE AND DATES COVERED
	February 1991	

4. TITLE AND SUBTITLE
Reflection of Incident Pressure Waves by Ribbed Panels

5. FUNDING NUMBERS

6. AUTHOR(S)
G. Maidanik and J. Dickey

7. PERFORMING ORGANIZATION NAME(S) AND ADDRESS(ES)
David Taylor Research Center
Codes 19 and 27
Annapolis, MD 21402

8. PERFORMING ORGANIZATION REPORT NUMBER
DTRC–91/006

9. SPONSORING /MONITORING AGENCY NAME(S) AND ADDRESS(ES)
David Taylor Research Center
Annapolis, MD 21402

10. SPONSORING /MONITORING AGENCY REPORT NUMBER

11. SUPPLEMENTARY NOTES

12a. DISTRIBUTION / AVAILABILITY STATEMENT
Approved for public release; distribution is unlimited.

12b. DISTRIBUTION CODE

13. ABSTRACT *(Maximum 200 words)*

The definitions of the reflection coefficients, in the absence of ribs and due to ribs, of an incident pressure wave on a plane at the surface of a ribbed fluid loaded panel are defined, examined, and computed. The incident pressure wave is described by a plane wave and by a collimated beam. The results of representative computations are displayed. Through these displays, some aspects of the influence on the reflection coefficients caused by changes in the parameters that describe the ribbed panel, the fluid loading, and the incidence are investigated. These aspects include wavenumber aliasings and symmetries in some of the terms and factors that compose the expressions for the reflection coefficients; the wavenumber of concern lies across the ribs. Aliasings are present, however, only when the separations between adjacent ribs are conditioned to be equal. Moreover, in some of these aliased terms and factors, symmetry is present only when the incidence obeys specific conditions. Disturbing either of these conditions tends to spoil the aliasing and/or the symmetries in these terms and factors. It is shown, however, that the aliasing and symmetry properties are invariant to changes in the parameters that describe the ribbed panel and/or the fluid loading to which it is subjected.

The role that the phenomenon of pass and stop bands (bands in reference to the frequency domain) plays in the reflection properties of ribbed fluid loaded panels is of particular interest here. It is illustrated that in the frequency ranges of pass bands, diffraction orders and aliasings tend to fade, and in the frequency ranges of stop bands they are enhanced. Fluid loading subdues the pass and stop bands, however, even substantial fluid loading does not eliminate these bands. Finally, the relationship between the reflection coefficients defined on the surface of the panel anon a control surface placed in the far-field is formulated and discussed.

14. SUBJECT TERMS	15. NUMBER OF PAGES
Pressure wave, Ribbed panel, Fluid loading, Aliasing, Symmetry properties, Pass and stop bands	49
	16. PRICE CODE

17. SECURITY CLASSIFICATION OF REPORT	18. SECURITY CLASSIFICATION OF THIS PAGE	19. SECURITY CLASSIFICATION OF ABSTRACT	20. LIMITATION OF ABSTRACT
Unclassified	Unclassified	Unclassified	Unlimited